1/130

Assessment of a Post-Waste Emplacement Geologic Setting Performance Measure

2/130

ASSESSMENT OF POST-WASTE EMPLACEMENT GEOLOGIC SETTING PERFORMANCE MEASURE

Prepared for

Nuclear Regulatory Commission
Contract NRC-02-93-005

Prepared by

R.T. Green
G.W. Wittmeyer
M.A. Muller
A.C. Bagtzoglou
E. King

Center for Nuclear Waste Regulatory Analyses
San Antonio, Texas

August 1994

3/130

ASSESSMENT OF A POST-WASTE EMPLACEMENT GEOLOGIC SETTING PERFORMANCE MEASURE

Systematic Regulatory Analysis (SRA) has identified Key Technical Uncertainties (KTUs) in the performance measure for the Geologic Setting (GS) described in 10 CFR 60.113(a)(2). The performance measure of the GS is commonly referred to as the Groundwater Travel Time (GWTT) rule. The KTUs identified in the GWTT rule are the determination of the extent of the "disturbed zone" and the identification of the "fastest path of likely radionuclide travel." The Nuclear Regulatory Commission (NRC) is investigating various approaches, such as rule making and/or staff guidance, for reducing these uncertainties. A post-waste emplacement performance measure was identified during previous studies by NRC and Center for Nuclear Waste Regulatory Analyses (CNWRA) staff as a means to reduce or remove uncertainties associated with the disturbed zone (IM 20-5702-451-402). Replacement of the current GWTT rule, which is for pre-waste emplacement conditions, with a post-waste emplacement performance measure has been assessed by staff at the CNWRA to determine the ability of the post-waste emplacement performance measure to reduce this uncertainty.

Since modeling will be used to demonstrate compliance with the performance measure, numerical exploration of any modification to the GWTT rule in 10 CFR 60.113(a)(2) is an essential component of investigations to test the actual utility of a performance measure for the GS. Accordingly, a post-waste emplacement performance measure for the geologic setting at a geologic high-level waste (HLW) repository has been assessed in this analysis using numerical simulations to track the trajectories of particles from a geologic HLW repository to the accessible environment. As defined by the Environmental Protection Agency (EPA) in 40 CFR Part 191, the accessible environment is located at ground surface and at a horizontal distance of 5 km from the boundary of the repository. Heat loads resulting from HLW buried at a geologic repository have been incorporated into the simulations to provide for post-waste emplacement conditions. Simulations of GWTT were conducted for only two geologic settings, a fully-saturated, fractured granite and a saturated/unsaturated uniform tuff. Based upon technical directions obtained from NRC staff, the analysis of the tuff case and that of the granite case were not conducted in exactly the same manner, but rather each analysis was tailored to address different aspects of the proposed post-waste emplacement rule. The additional computational complexity posed by adding the effects of heat to the fully saturated granite setting is modest when compared to the increased computational burden posed by modeling two-phase, nonisothermal flow in unsaturated tuff. Because nonisothermal saturated flow modeling is relatively straightforward, Monte Carlo simulation may be readily conducted to determine the distribution of travel times of groundwater particles from the repository to a compliance boundary in the granite geologic setting have been evaluated to test concepts of fastest path. In addition, the effect of persistent high or low permeability zones on arrival times has been incorporated into the granite setting cases. Incorporating the effect of heat on groundwater flow in the tuff geologic setting provided an opportunity to assess concepts relating to the disturbed zone particularly with regard to unsaturated media. However, owing to the complexity of the nonisothermal tuff setting calculations, only a limited number of simulations for this setting were conducted. The conceptual models, model dimensions, boundary, initial conditions, and physical property values for the granite and tuff models have been taken from letter report 20-5702-006-520-002 (Rice et al., 1993).

Prediction of thermally-induced groundwater movement through heterogeneous media is restricted by the computational requirements of incorporating both the physics of two-phase flow and the complexity of nonuniform media into the same simulation. Because of these computational demands, it is not currently feasible, nor is it anticipated to be feasible in the foreseeable future, to simulate groundwater flow in a

model that incorporates two-phase flow into a geologically complex model. Results reported in this document are from efforts to assess if geologically-reasonable predictions of groundwater flow driven by heat-generating high-level waste are computationally possible. Ramifications of the restriction due to the reasonable limit of available computation were realized during the conduct of these analyses when attempting to simulate groundwater flow driven by a repository heat source in a geologically-realistic model. A geologically-realistic representation could not be manifested in models which included two-phase flow mechanisms, thus the two-phase flow model predictions conducted in these analyses do not represent geologically-realistic settings. This absence of geologic realism in the models constructed to test post-waste emplacement assessments has led to the conclusion that crafting the GS performance measure as a post-waste emplacement measure is considerably less tenable than a pre-waste emplacement performance measure that does not incorporate nonisothermal flow. This report summarizes attempts by the CNWRA to invoke a post-waste emplacement based performance measure for the GS.

TECHNICAL APPROACH

The travel time of groundwater through porous media has been determined in these analyses by tracking neutrally-buoyant particles introduced into computed groundwater velocity fields. A total simulation time of approximately 100,000 yr was specified in these analyses to ensure that arrival characteristics such as multimodal particle arrival distributions will be detected. The groundwater flow regime was simulated for each of the two geologic settings, a fully-saturated fractured granite and a unsaturated/saturated homogenous tuff. The travel paths of neutrally-buoyant particles introduced into the predicted groundwater velocity fields were monitored and recorded. The fastest path of likely radionuclide travel was calculated using the arrival times of the particles at the compliance boundary. The particular calculational routine used to assess the post-waste emplacement performance measure for the granite setting was different than that used for the tuff geologic setting. Detailed descriptions of the computational methods and results for both geologic settings are contained in their respective sections. The utility of a post-waste emplacement geologic setting performance measure is assessed and discussed in the Conclusion section. Descriptions of possible future work to reduce uncertainty in the geologic setting performance measure are contained in the Recommendation section.

GRANITE GEOLOGIC SETTING

Repeated simulations were performed using PORFLOW-2.50 to estimate the GWTT distribution for a hypothetical mined geologic repository in a saturated, fractured granitic batholith. The conceptual model and parameter values assigned to this model were taken from Rice et al. (1993). This information is summarized in Appendix A. The repository was assumed to be 2,000 m in length and 10 m in height. It was also assumed that the pressure and temperature fields within the accessible environment are symmetric with respect to a plane normal to the width of the repository and could thus be modeled using a two-dimensional (2D) model. As shown in Figure 1, the spatial domain extends laterally 6 km up-gradient and 6 km down-gradient from the center of the repository, and vertically from 3 km below the repository to 1 km above the repository. Several highly conductive fault or fracture zones of variable thicknesses were assumed to exist near the repository.

Initial attempts to impose a uniform flow field across the model domain from left to right using prescribed head boundary conditions proved to be difficult. Under nonisothermal conditions, the vertically constant fictitious boundary heads caused water to circulate from the upper portion to the lower portion of each boundary. These difficulties were later traced to the manner in which PORFLOW-2.50 defines the

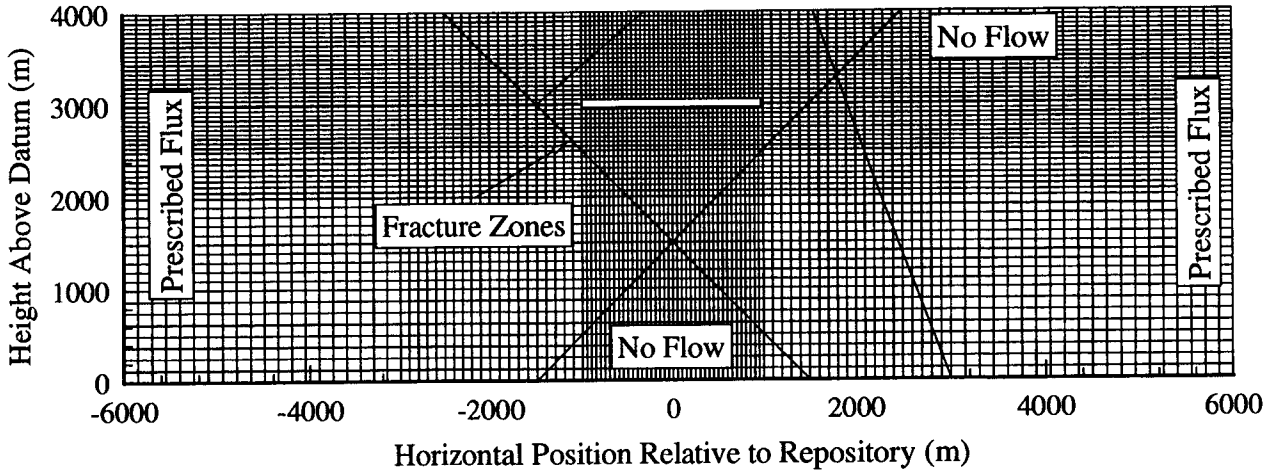

Figure 1. Computational mesh, boundary condition and fracture zone location for granite repository setting

reference temperature used to compute the buoyancy force. The velocity field should be independent of the reference temperature selected. However, within PORFLOW-2.50 one must ensure that if constant potential energy boundary conditions are used, the specified fictitious heads must reflect the vertical variation in the buoyancy force. For the travel time simulations reported here, a uniform flow field was achieved by imposing a prescribed flux of 4.2×10^{-12} m/s at the left and right boundaries of the model. The upper and lower boundaries were assumed to be impermeable. Initial hydraulic heads varied linearly from 4,050 m on the left to 4,000 m on the right. The background thermal field was wholly controlled by an assumed geothermal gradient of 0.025 K/m. Prescribed temperatures of 293.15 K and 393.15 K were specified at the top and bottom boundaries, respectively. Temperatures along the right and left boundaries were assumed to vary linearly from 393.15 K to 293.15 K from bottom to top. It should be noted that the use of prescribed temperature condition instead of zero heat flux conditions on the vertical boundaries may cause the model to underestimate the effect of repository heating on the flow regime. Initial temperatures reflect the assumed geothermal gradient.

The hydraulic conductivities of the granite matrix and backfilled repository were assumed to be 1.0×10^{-9} m/s and 1.0×10^{-8} m/s, respectively. The coefficient of elastic storage for all materials was set to 1.0×10^{-8}. The porosities of the granite matrix, backfilled repository and fracture zones were assumed to be 0.01, 0.1 and 0.1, respectively. The bulk density for all material types was 2,670 kg/m^3. Specific heat capacity and thermal conductivity for all material types were 990 J/kg-K and 3.2 W/m-K, respectively. The temperature dependence of fluid density was defined by a simple power law. The specific heat capacity, thermal conductivity and compressibility of the fluid were 4,180 J/kg-K, 0.6 W/m-K, and 4.5×10^{-10} Pa^{-1}, respectively.

The computational grid shown in Figure 1 consists of 7,139 nodes, with 121 nodes in the horizontal direction and 59 in the vertical direction. As can be seen in Figure 1 the rectilinear mesh is increasingly refined near the repository in order to accommodate large fluid pressure and temperature gradients that may develop. The time-dependent thermal load at the repository is based on estimates by Brandshaug (1991) for the thermal decay of 40 percent BWR and 60 percent PWR spent fuel and an initial areal thermal loading of 14.085 W/m^2 (57 kW/acre).

For the granite geologic setting it is assumed that highly permeable fault or fracture zones provide the fastest path to the accessible environment for any particles exiting the repository. The likelihood that a particle will reach the accessible environment depends both on the proximity of the repository to a fault or fracture zone and the width and hydraulic conductivity of that zone. It was assumed for this study that through the process of site characterization the locations of most highly conductive zones should be identified. However, site characterization may not provide definitive estimates of the widths and hydraulic conductivities of these zones. Therefore, while the location and orientation of the fault or fractures zones need not be treated probabilistically in this GWTT analysis, uncertainty regarding their width and hydraulic conductivity requires the application of appropriate Monte Carlo procedures. Although not included in this analysis, the effects of varying the hydraulic properties of the granite matrix and backfilled repository, as well as the initial and boundary conditions on the GWTT distribution should also be investigated in future efforts.

For this GWTT analysis a single conceptual model of the location, length and orientation of the fault or fractures zones was used. As shown in Figure 1, the four fault or fracture zones are located near the repository horizon but do not intersect it. However, these fault or fracture zones do transect areas immediately above, below, upstream and downstream of the repository horizon so that fluid particles that exit the repository may be entrained and conveyed to the accessible environment. The latin hypercube sampling (LHS) program developed by Inman and Shortencarier (1984) was used to generate realizations of the four fault zones width and hydraulic conductivity. The width was assumed to be uniformly distributed with lower and upper bounds of 0.5 m and 5.0 m, respectively. The hydraulic conductivity for each fault or fracture zone was assumed to be lognormally distributed with mean -13.8 m/s and standard deviation 3.5 m/s. These parameters result in 0.999 and 0.001 exceedence frequencies that correspond to fracture zone hydraulic conductivities of 2.11×10^{-11} m/s and 4.88×10^{-2} m/s, respectively. Experience indicates that if LHS is used to generate a random vector of length n, reasonably accurate variance estimates can be obtained by generating a total of $4n/3$ realizations. For this problem LHS is used to generate four fracture zone widths and four values of hydraulic conductivity to fill a random vector of length 8 thus, using the $4n/3$ rule, only 11 realizations are required. Because 20 realizations of the fault or fracture zone properties were generated, the sample statistics should accurately reflect the underlying distributional assumptions. Examples of temperature and fictitious head contours at 490 yr are shown in Figures 2 and 3, respectively. One must be cautioned against using the fictitious head contours to infer the direction of the flow field since the effects of buoyancy are not included. Example of particle trajectories for the 99,990 yr period are superimposed on the temperature contours shown in Figure 2. Figures 4 and 5 depict the velocity field for the nonisothermal case at 490 yr with streamlines emanating from the horizontal centerline of the repository and from the upstream boundary, respectively. Because the heat load varies with time the velocity field is transient and the streamlines shown in Figure 5 are not coincident with the particle trajectories shown in Figure 3.

Travel times for each realization were determined by releasing 100 particles distributed uniformly along the length of the repository and tracking the particle trajectories using PORFLOW-2.50's particle tracking algorithm. Additional software was developed to post-process the particle trajectory data and determine

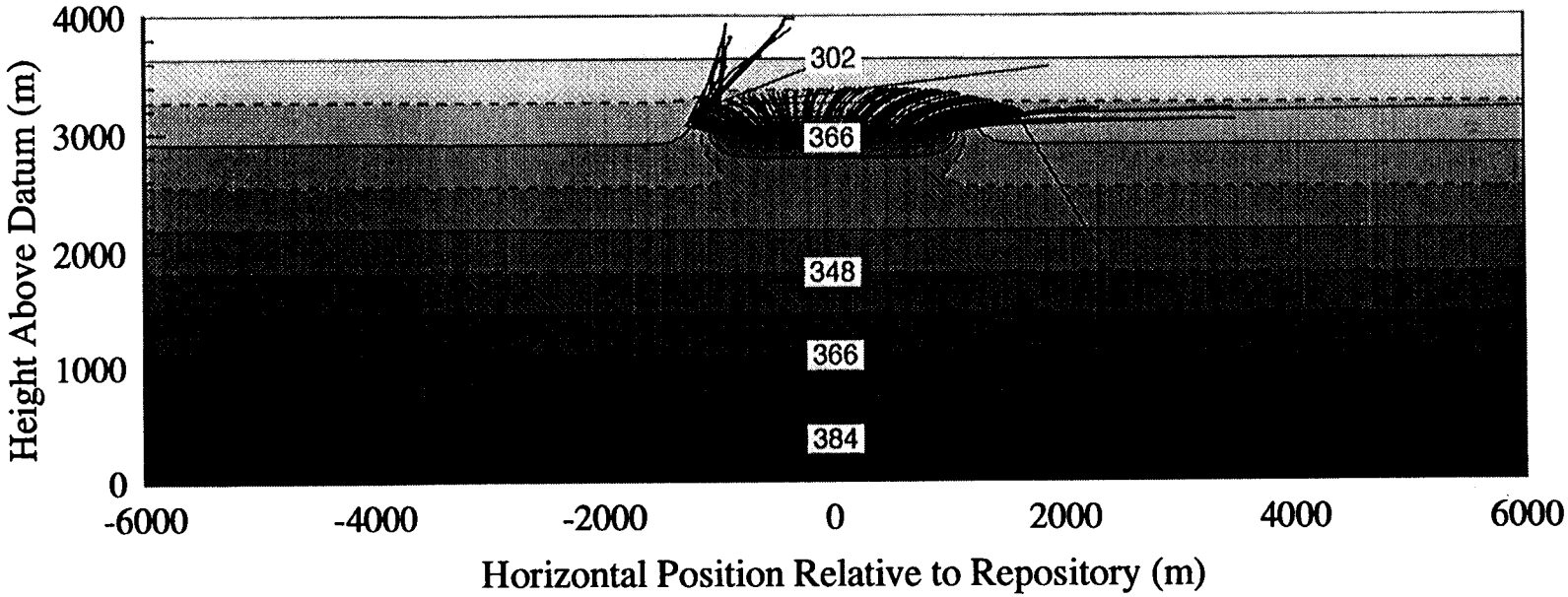

Figure 2. Sample temperature contours for the granite repository setting at time 490 yr with sample particle trajectories for the 99,990 yr simulation period. Labels on contour lines are in Kelvins.

5/30

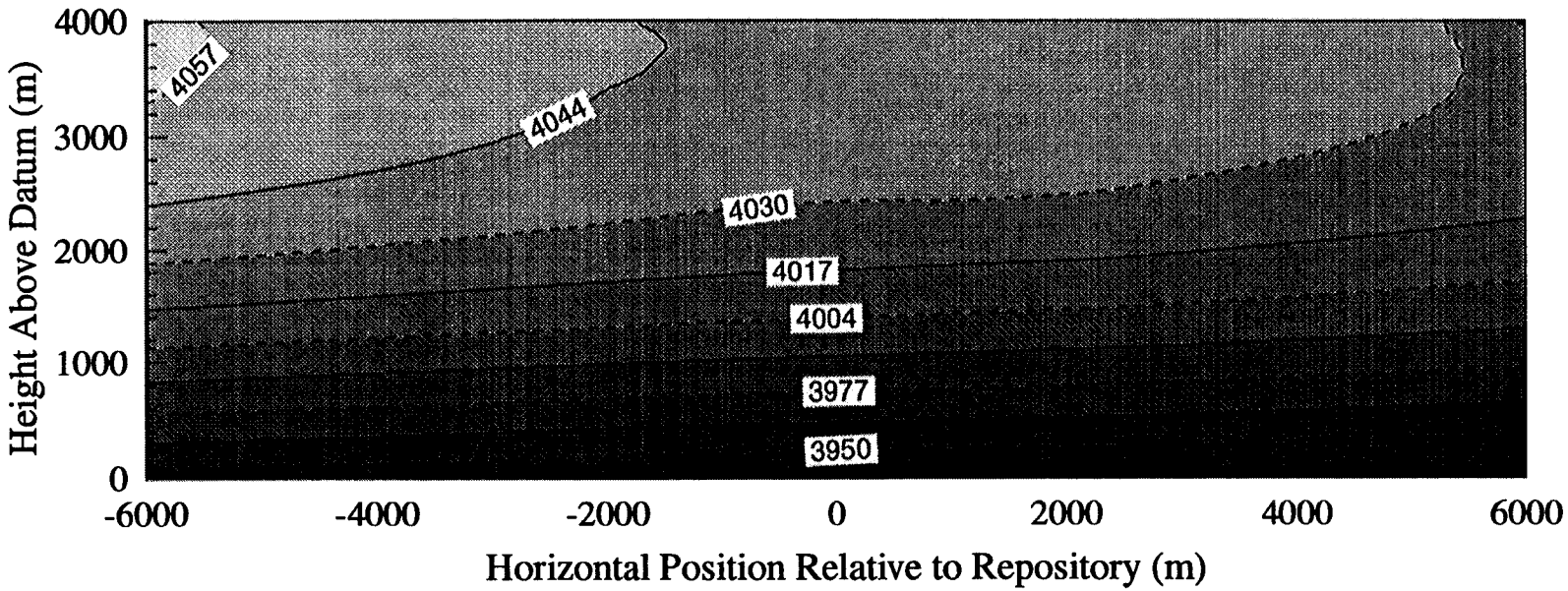

Figure 3. Sample fictitious hydraulic heads for the granite repository setting at time 490 yr. Labels on contours are in meters of water and are defined in terms of the density of water at the reference temperature of 300 Kelvins.

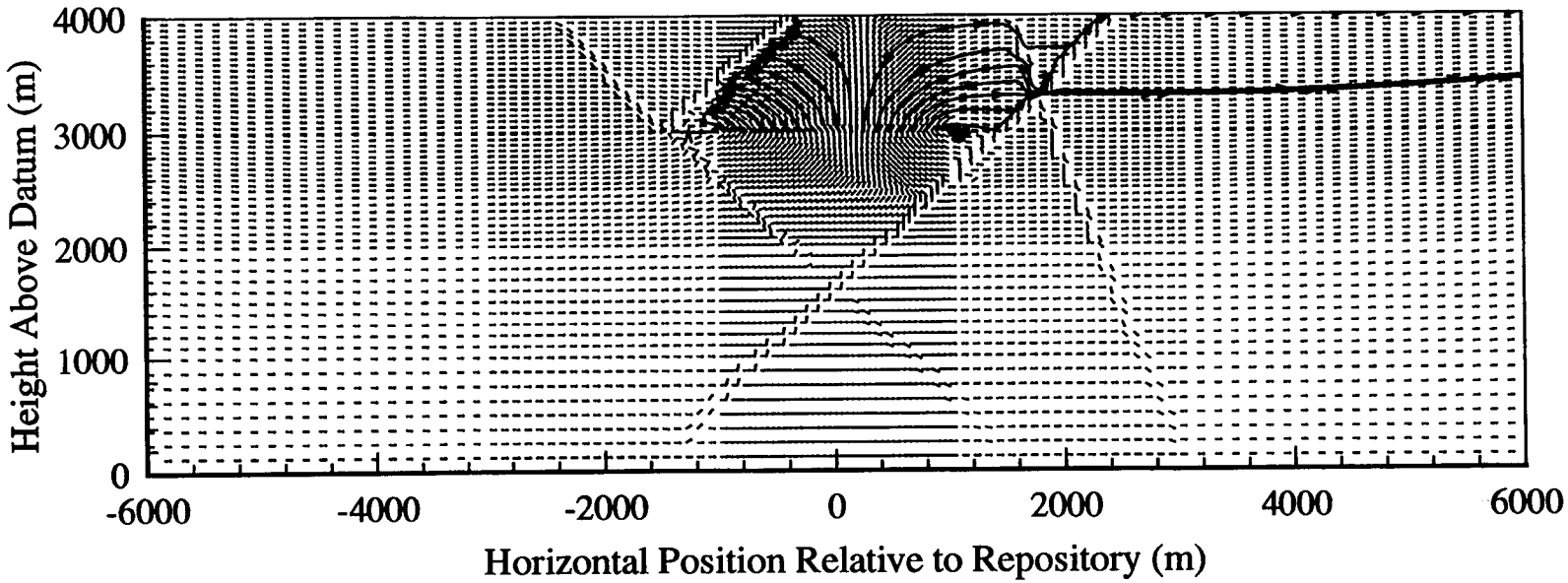

Figure 4. Sample velocity field for the granite repository setting at time 490 yr with streamlines emanating from the horizontal centerline of the repository.

4/30

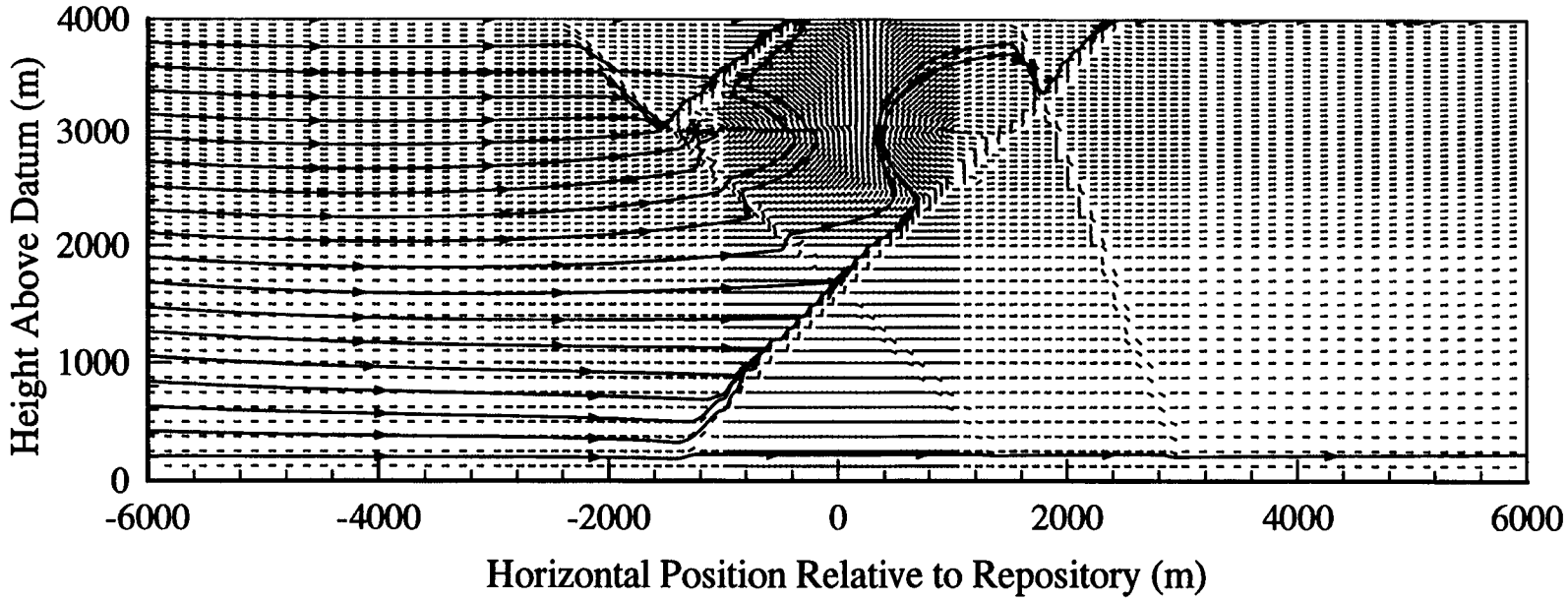

Figure 5. Sample velocity field for the granite repository setting at time 490 yr with streamlines emanating from the upstream boundary.

travel times to each of four rectangular compliance boundaries centered about the repository and one rectangular compliance boundary corresponding to the accessible environment. The locations of the five rectangular compliance boundaries, referred to as numbers 1 through 5, are shown in Figure 6. The widths and heights of the smallest to the largest rectangular compliance boundaries are 2,100 m by 50 m, 2,200 m by 100 m, 3,000 m by 200 m, 6,000 m by 1,000 m, and 12,000 m by 4,000 m, respectively.

Travel time statistics for the case that includes the effect of repository heating are shown in Table 1 for the 19 realizations which yielded meaningful results. Of the 1,900 particles released, 1,861 produced valid trajectories, and 1,857 of these particles reached the first compliance boundary during the 99,990 yr simulation period. However, only 13 particles reached the accessible environment during the simulation period. Because the simulations were performed over a time period that was not long enough to permit all particles to cross all compliance boundaries, the travel time statistics for each compliance boundary cannot be easily compared. However, in the case of compliance boundaries 1, 2, and 3, where the number of particles reaching the compliance boundaries are roughly the same (1,857, 1,850, and 1,815, respectively), some conclusions may be drawn from comparison of the travel time statistics. The minimum travel times to the three closest compliance boundaries are 3,688, 4,614 and 7,311 yr, respectively. Histograms of travel times to compliance boundaries 1, 2, and 3 are shown in Appendix B in Figures B-1, B-2, and B-3, respectively. All three histograms appear to be unimodal and each has a sample mean that is very close to the sample median, although the distributions do change from being positively skewed near the repository to being negatively skewed farther from the repository. One might have expected that the travel time distributions for a porous-fractured medium would be multimodal, perhaps reflecting the vastly different velocities experienced by particles in the granite matrix and from those in the fractures. This is clearly not the case for the travel time distributions shown in Figures B-1, B-2 and B-3. Additional analyses show that more than 90 percent of the particles that cross compliance boundaries 1, 2, and 3 are driven upward by thermal buoyancy effects, cross the top of each compliance boundary and thus do not become entrained in the fracture zones. As shown by the histograms in Figures B-4 and B-5, the travel time distributions for compliance boundaries 4 and 5 are multimodal. This presumably occurs because a larger percentage of the particles reaching these compliance boundaries are conveyed through the fault or fracture zones.

In order to assess what effect heating had on the flow regime, the nominal case with no repository heating was also investigated. Travel time statistics for the nominal case are shown in Table 2 for all 20 realizations. Due to the absence of thermal buoyancy, far fewer of the 1,989 valid particle trajectories obtained from these realizations actually crossed any of the five compliance boundaries during the 99,990 yr simulation period. As was the case for the nonisothermal realizations, far fewer particles crossed the two outermost compliance boundaries than crossed the three innermost boundaries. The number of particle trajectories that crossed compliance boundaries 1, 2 and 3, were 324, 300 and 202, respectively. The minimum travel times to compliance boundaries 1, 2, and 3 were 5,201, 7,319, and 11,948 yr, respectively. These minimum travel times are significantly larger than those obtained for the nonisothermal case, which again illustrates the pronounced effect that thermal buoyancy has on the flow field. Histograms of travel times to compliance boundaries 1, 2, and 3 are shown in Figures B-6, B-7, and B-8, respectively. In contrast to the travel time distributions recorded at the three closest compliance boundaries for the nonisothermal case, these distributions appear to be more multimodal. In addition, the distributions for the isothermal cases have significantly larger standard deviations than do those for the nonisothermal case. The larger spread of the travel time distributions, as well as their pronounced multimodality, can be explained by the fact that between 19 and 29 percent of the particles crossed the top boundaries, and 64 to 77 percent crossed the downstream or right boundaries. A greater percentage of these particles crossed the compliance boundaries on the downstream side than did for the

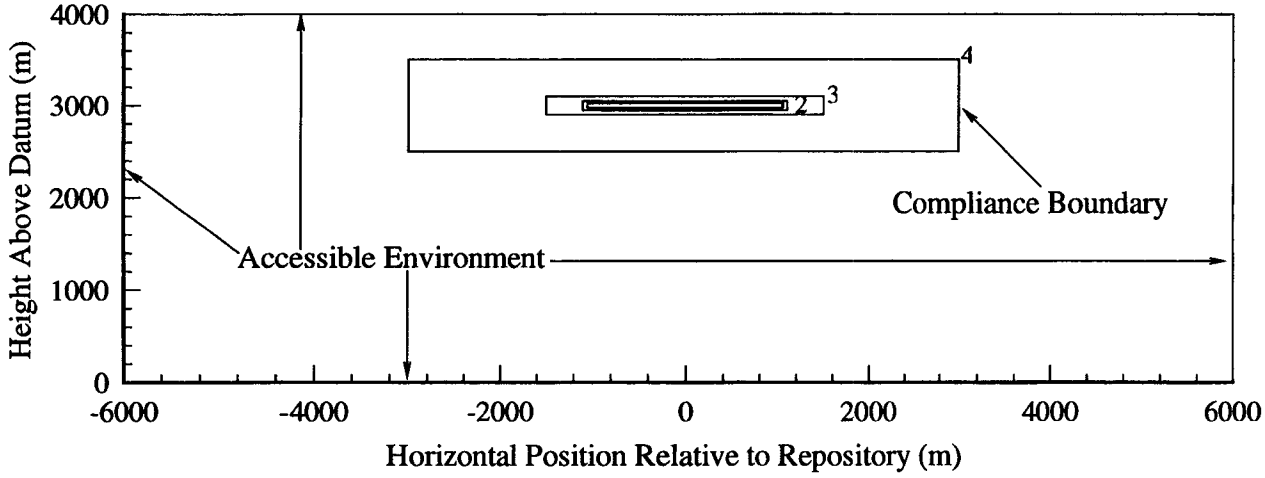

Figure 6. Location of compliance boundaries

nonisothermal case due to the absence of vertical gradients induced by thermal buoyancy. Due to the location of the fracture zones one might expect that particles that were transported downstream by the regional flow field would eventually be entrained in a fracture and rapidly transported to the accessible environment. Only 4 particles reached the accessible environment for the isothermal case whereas 13 did for the nonisothermal case. However, the minimum travel time to the accessible environment for the isothermal case was 51,629 yr as compared to 88,283 yr for the nonisothermal case. Statistics for the minimum travel times recorded for each of the 19 realizations performed for the nonisothermal case and each of the 20 realizations performed for the isothermal case are shown in Tables 3 and 4, respectively. Distributions of the minimum travel times are shown by histograms in Figures B-9 a-d, and B-10 a-d.

TUFF GEOLOGIC SETTING

Heat and mass transfer at a HLW repository located in partially-saturated tuff overlying a saturated zone consisting of tuff underlain by a carbonate layer has been simulated using VTOUGH 4.1 to determine the GWTT from the repository to the accessible environment (Pruess, 1987, Nitao, 1989). The conceptual model and parameter values assigned to this model were taken from Rice et al. (1993). This information is summarized in Appendix C. The model consisted a vertical 2D cross section having a vertical dimension of 1,625 m and extending laterally for a distance of 14 km. An arbitrary 25 m thick layer was placed at the top and bottom of the model to provide the means to establish boundary conditions, thus creating a total model thickness of 1,675 m. The model consisted of a uniform tuff to a depth of 1,575 m with a 50 m thick horizontally uniform carbonate layer located at the base. The water table was located at a depth of 550 m below ground surface or 250 m below the repository.The model grid had 1,960 nodes consisting of 70 equally-spaced (at 200 m) nodes in the horizontal direction and 28 nodes in the vertical direction with a more refined horizontal grid at the repository horizon (Figure 7). The repository

Table 1. Travel time statistics: Repository heat load

	Compliance Boundary				
	1	2	3	4	5
Minimum Travel Time (years)	3,688	4,614	7,311	11,045	88,283
Maximum Travel Time (years)	91,389	98,303	99,742	99,946	99,982
Median Travel Time (years)	37,189	48,096	57,240	69,064	98,424
Mean Travel Time (years)	38,133	48,848	57,992	63,094	97,247
Standard Deviation (years)	9,140	11,546	12,273	26,609	28,275
CVAR	0.24	0.24	0.21	0.42	0.29
Skewness	0.66	0.08	−0.24	−0.40	0.00
Number of Particles	1,857	1,850	1,815	188	13

8/30

Table 2. Travel time statistics: No repository heat load

	Compliance Boundary				
	1	2	3	4	5
Minimum Travel Time (years)	5,201	7,319	11,948	15,107	51,629
Maximum Travel Time (years)	99,992	99,922	99,944	99,246	95,386
Median Travel Time (years)	60,135	63,231	71,859	53,809	62,447
Mean Travel Time (years)	58,851	61,737	68,701	57,446	74,754
Standard Deviation (years)	24,098	24,279	21,307	25,578	48,025
CVAR	0.41	0.39	0.31	0.45	0.64
Skewness	-0.18	-0.18	-0.50	0.12	0.00
Number of Particles	324	300	202	54	4

Table 3. Statistics of minimum travel time: Nonisothermal case.

	Compliance Boundary				
	1	2	3	4	5
Minimum Travel Time (years)	3,688	4,614	7,311	11,045	88,283
Maximum Travel Time (years)	45,381	57,856	67,171	97,138	99,836
Mean Travel Time (years)	23,919	30,246	44,236	53,578	94,059
Median Travel Time (years)	16,808	20,325	39,847	52,447	94,059

9/30

Table 4. Statistics of minimum travel time: Isothermal case.

	Compliance Boundary				
	1	2	3	4	5
Minimum Travel Time (years)	5,201	7,319	11,948	15,107	51,629
Maximum Travel Time (years)	72,744	85,916	65,545	89,113	89,553
Mean Travel Time (years)	23,974	28,182	48,555	54,114	70,591
Median Travel Time (years)	20,543	24,368	48,329	55,975	70,591

10/30

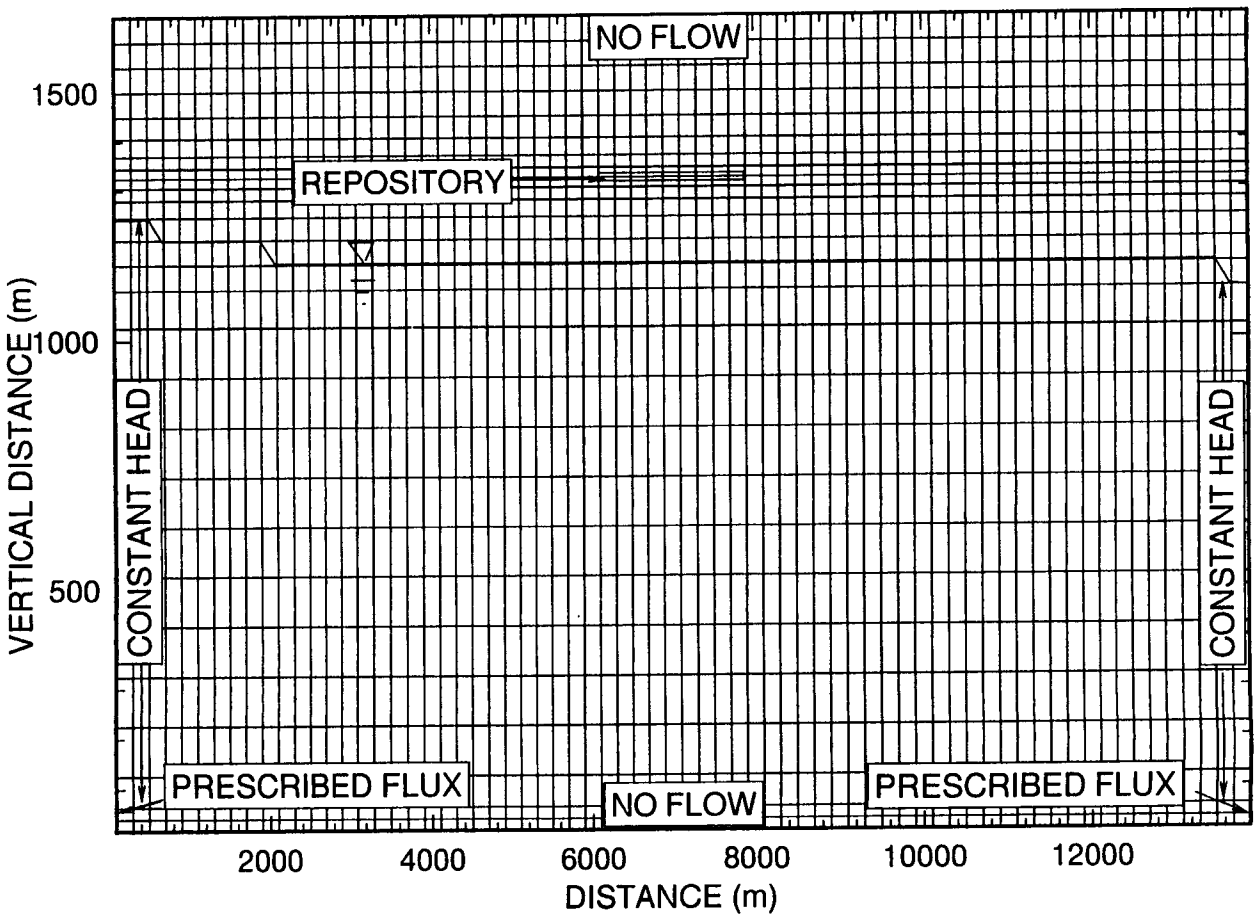

Figure 7. Computational mesh for tuff geologic setting. Initial groundwater surface is denoted with a ∇.

was symmetrically located midway between the sides of the model at a depth of 300 m and had an assumed height of 20 m and length of 2 km. A repository thickness (and minimum node distance) of 20 m was assigned to maintain a maximum nodal aspect ratio of 10 in the finite difference grid. The accessible environment was established as a vertical surface located 5 km from the edge of the repository. The vertical boundaries of the model were located 6 km from the edge of the repository. An extra kilometer, in addition to the 5 km distance from the repository to the accessible environment as specified in 40 CFR Part 191, was added to both ends of the model to help combat difficulties associated with the free-surface boundary near the model boundaries, and with the formation of a convection cell the size of the model domain.

The top and bottom of the model domain were assumed to be impermeable. The vertical boundaries located in the saturated zone of the tuff layer were prescribed as constant head to establish a regional groundwater gradient. The hydraulic head in the saturated zone at the up-gradient boundary of the model was maintained 40 m greater than the hydraulic head 6 km down-gradient from the repository, thus imposing a regional hydraulic gradient of 0.0029. A flux of 0.2 $m^3/5\text{-}m^2$ was prescribed for the carbonate layer (positive on the left and negative on the right) to induce horizontal flow to be consistent with the conceptual model identified in Rice et al. (1993). The top (at 283 K), basal (at 323 K) and side (at a linear gradient between the top and base) boundaries were maintained as constant temperature boundaries to impose an assumed geothermal gradient of 0.025 K/m. All four boundaries were held at constant temperature to limit the effects of the convection cells.

The modeled medium was treated as a composite medium (Klavetter and Peters, 1986, Nitao, 1988). In this characterization, bulk permeability and bulk liquid hydraulic conductivity were volume-averages of the respective fracture and matrix properties of the medium. The bulk permeability can be written in terms of the matrix and fracture saturated hydraulic conductivities, K, relative permeabilities, k, and porosities, ϕ, as

$$k_{rl}^{b}=\frac{\left[K_f k_{rl}^{f}\phi_f+K_m k_{rm}^{m}(1-\phi_f)\right]}{K_b} \tag{1}$$

where b, f, m and r denote bulk, fracture, matrix and relative, respectively. Similarly the bulk liquid hydraulic conductivity is expressed

$$K_b=K_f\phi_f+K_m(1-\phi_f) \tag{2}$$

Using these relationships, the tuff is assigned a bulk permeability of 1.8×10^{-14} m^2 (equivalent to a hydraulic conductivity of 1.75×10^{-7} m/s) and the carbonate layer a value of 1.8×10^{-6} m^2 (17.6 m/s). Both were assigned porosities of 0.11. Since a portion of the tuff is less than fully saturated, a composite van Genuchten-Mualem model was selected to describe the unsaturated hydraulic characteristic properties. These values are 5.8004×10^{-7} Pa^{-1}, 1.3147×10^{-4} Pa^{-1} for α, 1.798, and 4.23 for β for the matrix and the fractures, respectively (Klavetter and Peters, 1986). Bulk density of the tuff and carbonate units was 2,580 kg/m^3. The carbonate unit was assigned a thermal conductivity of 2.3 W/m-K. The thermal conductivity of the tuff unit varied linearly from 2.3 W/m-K when fully saturated to 1.7 W/m-K when dry. Both units had a specific heat of 840 J/kg-K.

Initial groundwater potential conditions were determined by simulating heat and mass transfer in the naturally-occurring system for 10,000 yr. The naturally-occurring system exhibited heat and mass transfer

due to a geothermal gradient and the other specified boundary conditions but in the absence of heat generated by a repository. Initial temperature and pressure contours and location of the water table surface determined after 10,000 yr of simulation are illustrated in Figure 14. Numerical simulation difficulties associated with heat and mass transfer predicted for a system with finite boundaries, uniform media properties and a geothermal gradient are apparent in the temperature contours. As illustrated, a counter-clockwise convection cell formed with cell dimensions equal to the saturated portion of the model. The portion of the convection cell that caused a distortion of the groundwater free surface is beyond the region of interest of the model (i.e., beyond the accessible environment located 5 km from the repository) and is not addressed in this analysis. The convection cell which is apparent at 10,000 yr is even more developed at later simulation times. The effect of the model-scale convection cell on the liquid-flow regime is evident in the flow regimes simulated by this model even in the presence of heat generated by the repository. This effect becomes increasing pronounced for larger permeabilities, an observation consistent with the Rayleigh Number, a dimensionless term whose value increases with the propensity for formation of a convection cell, in which the permeability appears in the numerator.

Groundwater and heat flow was then simulated for 100,000 yr, assigning as the initial conditions those predicted at the conclusion of the 10,000 yr simulation. These flow regimes were predicted for an areal heat load of 114 kW/acre (Brandshaug, 1991). This areal heat load corresponds to the proposed extended-dry repository (Buscheck and Nitao, 1992), which is twice the areal heat load cited in the Site Characterization Plan (DOE, 1988). This larger areal heat load was selected for these analyses to enhance the thermally-induced moisture redistribution. This was viewed as the most conservative approach,since the disturbed zone has a much greater areal extent at 114 kW/acre than at 57 kW/acre.

The lateral width of the repository was maintained at 2,000 m even though the areal heat load was doubled from 57 to 114 kW/acre. Although it could be inferred that the total heat generated at the repository was also doubled, the interpretation here is that the repository total heat load has remained at SCP specified levels but that the repository length has been reduced by half. This interpretation weakens the 2D assumption however, it was determined that this interpretation was again conservative.

Predictions of temperature at 100, 500, and 1,000 yr and at 10,000, 50,000, and 100,000 yr for an areal heat load of 114 kW/acre are illustrated in Figures 9 and 10 respectively. Two observations can be made from these figures. First, the thermal effect of the HLW penetrates well into the saturated zone within 1,000 yr after waste emplacement, and that thermal effects can be detected as deep as the base of the tuff, 1,200 m below the repository horizon, by 100,000 yr. Second, the presence of the convection cell becomes particularly prominent by 10,000 yr into the simulation.

Figure 11 presents the 97 °C isotherm at all times (50, 100, 500 and 1,000 yr) in which this isotherm was observed in the simulations. The 97 °C isotherm is of interest because 97 °C is the boiling temperature predicted for water at the repository horizon. The area within the 97 °C contour is essentially dry. The absence of temperatures in excess of 97 °C for times less than 50 yr or greater than 1,000 yr is, in part, attributed to the coarseness of the grid size (e.g., 20 by 200 m). However, the primary reason that 97 °C is not exceeded at later times is that the heat source term experiences a nearly exponential decay in strength from the initial time of the simulation. Insufficient heat is generated, even in an extended-dry repository, to maintain temperatures above 97 °C for periods approaching 5,000 yr.

The size of the region contained within the 97 °C isotherm expands during the period of simulation from a total vertical extent of approximately 75 m at 50 yr, to nearly 300 m at 1,000 yr. The lateral extent of the dry-out zone, which reached a maximum of about 80 m beyond the repository, was less than the

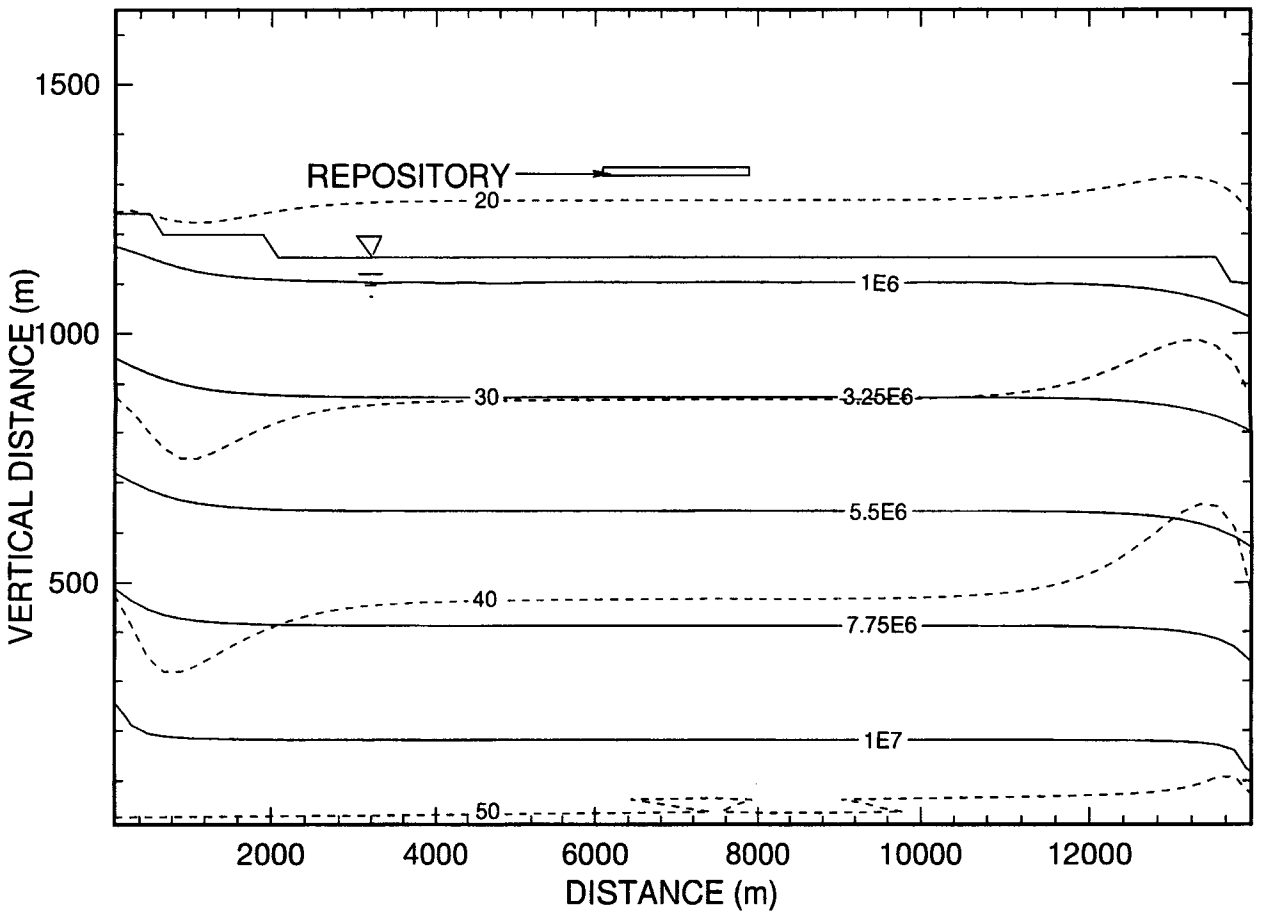

Figure 8. Temperature (C) (dash) and pressure (Pa) (solid) of tuff geologic setting after 10,000 of simulation

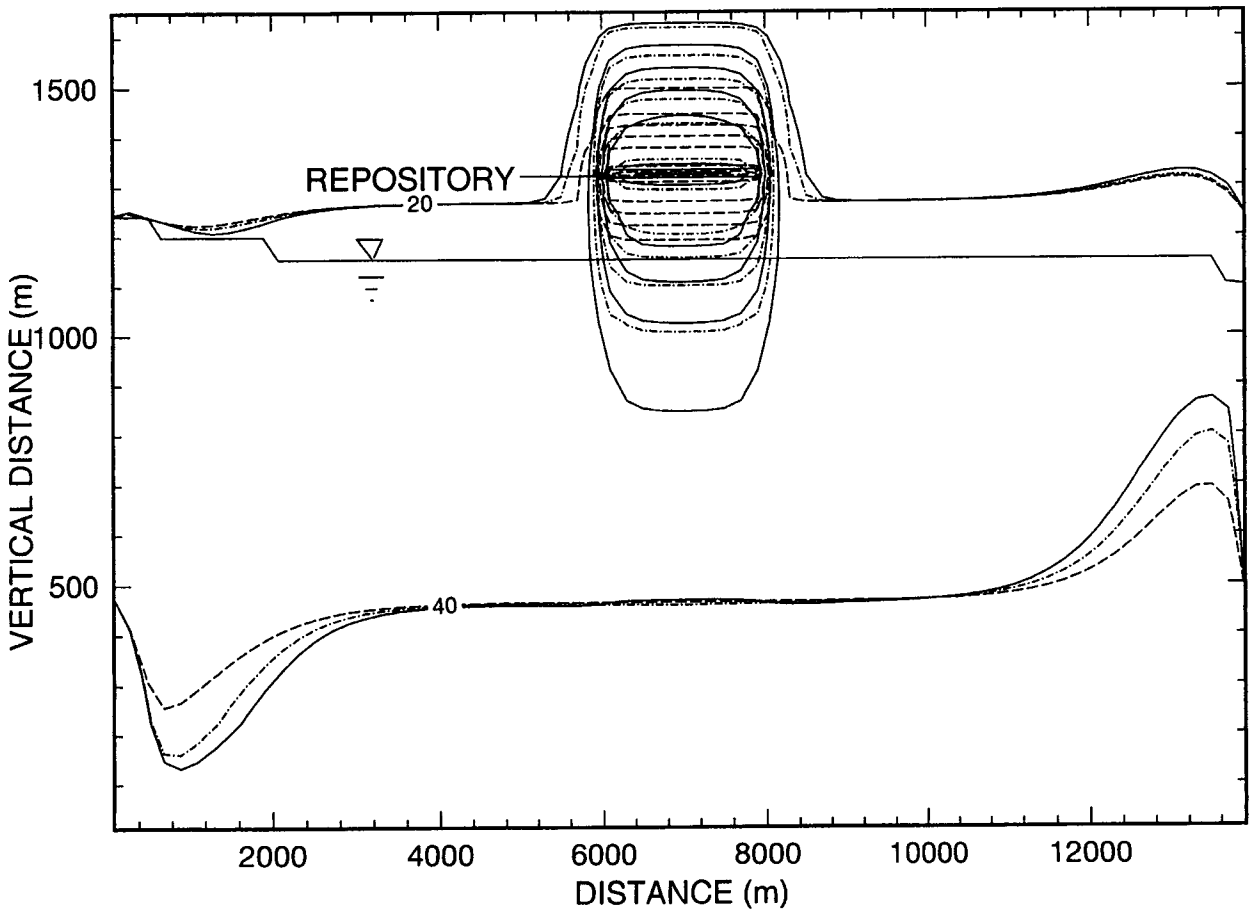

Figure 9. Temperature (C) after 100 (dash), 500 (dot-dash) and 1,000 (solid) yr of simulation. Maximum temperature is 146, 140 and 129 °C at 100, 500 and 1,000 yr, respectively. Contour interval is 20 °C.

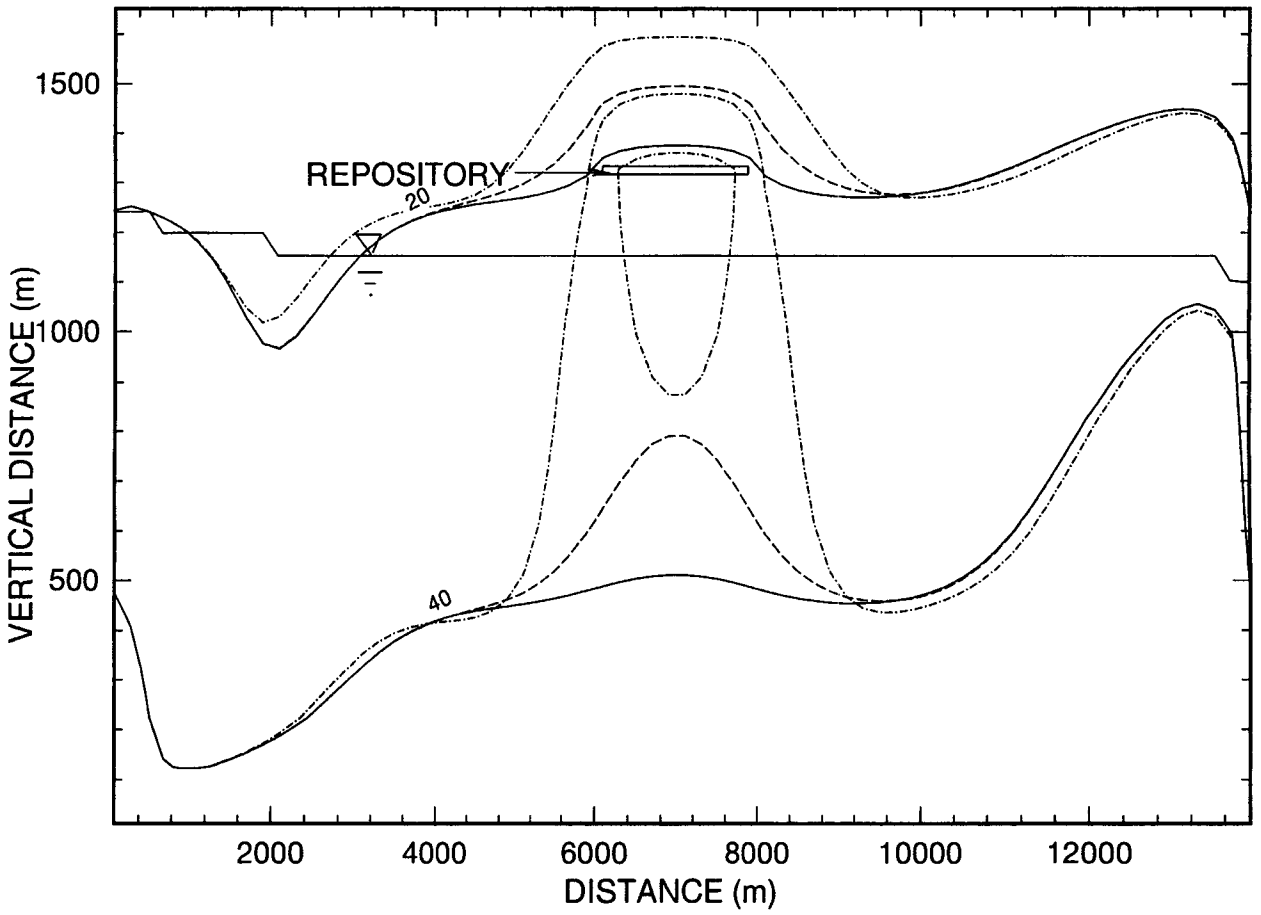

Figure 10. Temperature (°C) after 10,000 (dot-dash), 50,000 (dash) and 100,000 (solid) yr of simulation. Maximum temperature is 65, 50 and 50 °C at 10,000, 50,000 and 100,000 yr, respectively. Contour interval is 20 °C.

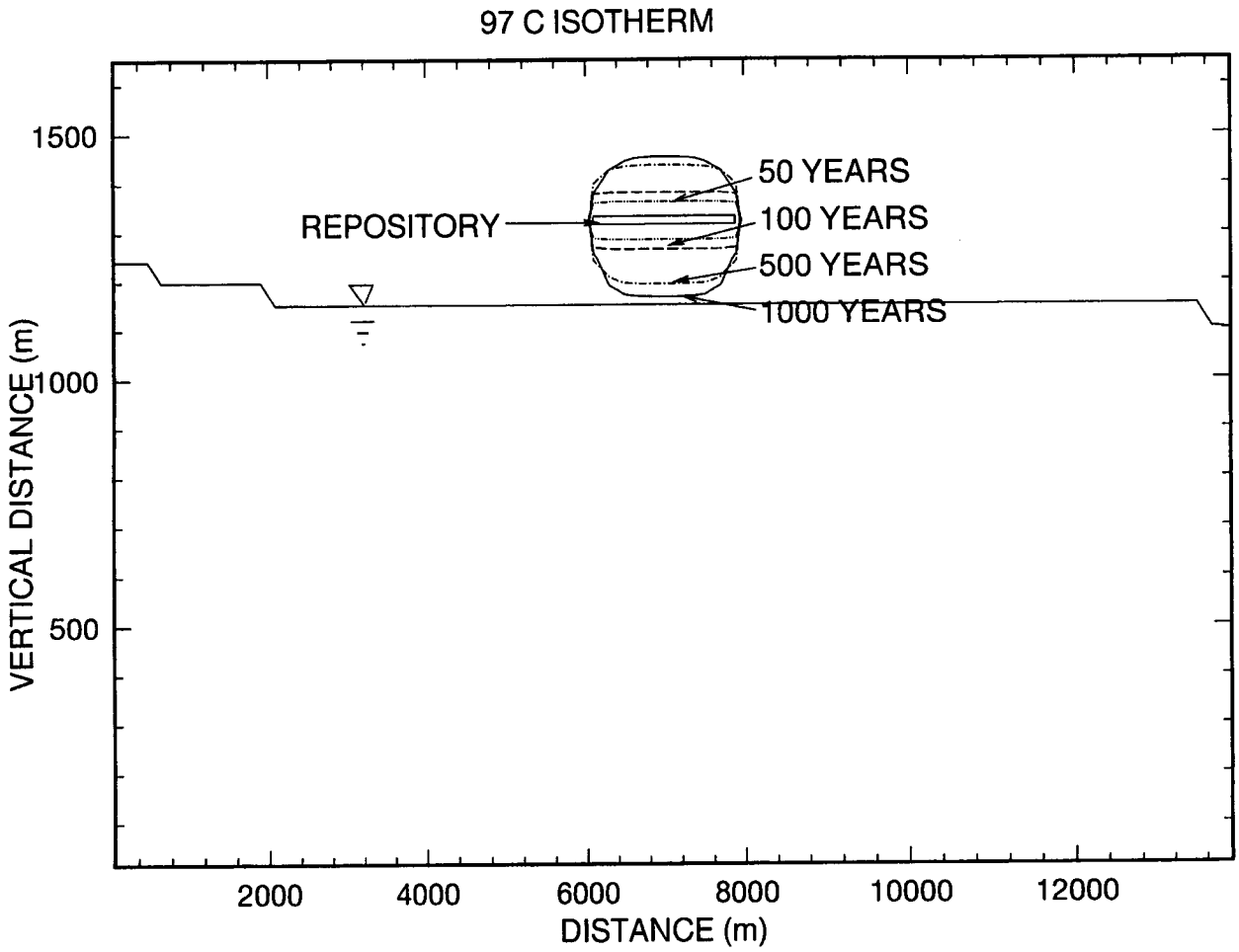

Figure 11. Extent of the 97 °C isotherm at 50 (dot-dot-dash), 100 (dash), 500 (dot-dash) and 1,000 (solid) yr in the simulation

vertical extent at all times. These simulations indicate that the vertical extent of the dry-out zone comes within 20 m of the water table during the 1,000 yr simulation.

A total of 6,000 particles was introduced into the simulated velocity fields at the repository and tracked using SLIM, a particle tracking code (Bagtzoglou and Muller, 1994). Initially the effect of dispersion was included in the particle tracking simulations with both longitudinal and transverse dispersion assumed to be 5 m. Since simulations including dispersion were essentially equivalent to simulations with only advection, dispersion was neglected from the particle tracking exercises to reduce the computational demands of the analyses. The location of the particles initially introduced at the repository after 100,000 yr of tracking is illustrated in Figure 12. As evidenced in this figure, none of the particles moved significantly from the repository horizon.

The lack of movement of any of the 6,000 particles away from the repository after 10,000 yr of simulation is an indication of the limitation in predicting groundwater flow near the repository when assuming a uniform, homogeneous medium. The assumption of a uniform heat source in a perfectly uniform, homogeneous medium causes formation of a capture zone encapsulating the repository. The capture zone is created by the heat load which vaporizes water at the repository, the resultant water vapor pressure gradient drives the generated water vapor away from the repository to a distance where the vapor condenses at lower temperatures. A uniform, symmetric liquid water capture zone encapsulating the repository is formed by the flow of liquid water toward the heat source in response to the liquid water pressure gradient formed by the relative locations of vaporized and condensed water. It is the formation of this capture zone that prohibits the movement of particles away from the repository for as long as the capture zone persists. The formation of a capture zone that effectively retains virtually all particles at the repository is not believed to be geologically realistic. In reality, nonuniformity in the heat source, heterogeneities in the medium and the presence of persistent flow features will provide avenues for liquid water movement throughout the duration of the repository design period, particularly for the movement of water originating from zones of high water saturation above the repository downward through and past the repository horizon.

A second set of particles was tracked using the same velocity fields presented above, except in this instance the 6,000 particles were introduced at a 2,000 m wide horizon located 50 m below the repository. Again, none of the particles had any noticeable movement during the 100,000 yr simulation except for some upward movement toward the repository, further evidence of the capture zone (Figure 13). In the third and final set of particle tracking simulations, the 6,000 particles were introduced in a 2,000 m wide horizon at a location 300 m directly below the repository. A significant difference in the third case was that the particles were introduced in the saturated zone at a depth of about 100 m below the water table. In this case there was noticeable movement in the particles. By 1,000 yr into the simulation the lead particles were transported less than 50 m downward in the vertical direction (Figure 14). By 5,000 yr, the lead particles were transported 650 m vertically downward from the point where they were introduced into the subsurface (Figure 15). The particles were transported downward in the region directly below the repository. The direction of groundwater flow in this region was determined to be downward for the first 1,000 yr of the simulation, then switching to upward by 5,000 yr (CNWRA, 1994). There was no significant horizontal component to either the upward or downward flow regimes. The upward and downward flow patterns located directly below the repository are parts of large convection cells with dimensions equal to those of the model. The large cells formed, in part, due to the homogeneous, uniform nature of the model. Rayleigh numbers, a dimensionless term used to describe the onset of convection, are larger in ideal settings where there is an absence of horizontally-oriented layers or seams with permeability significantly less than the bulk of the medium. Such layers are

14/30

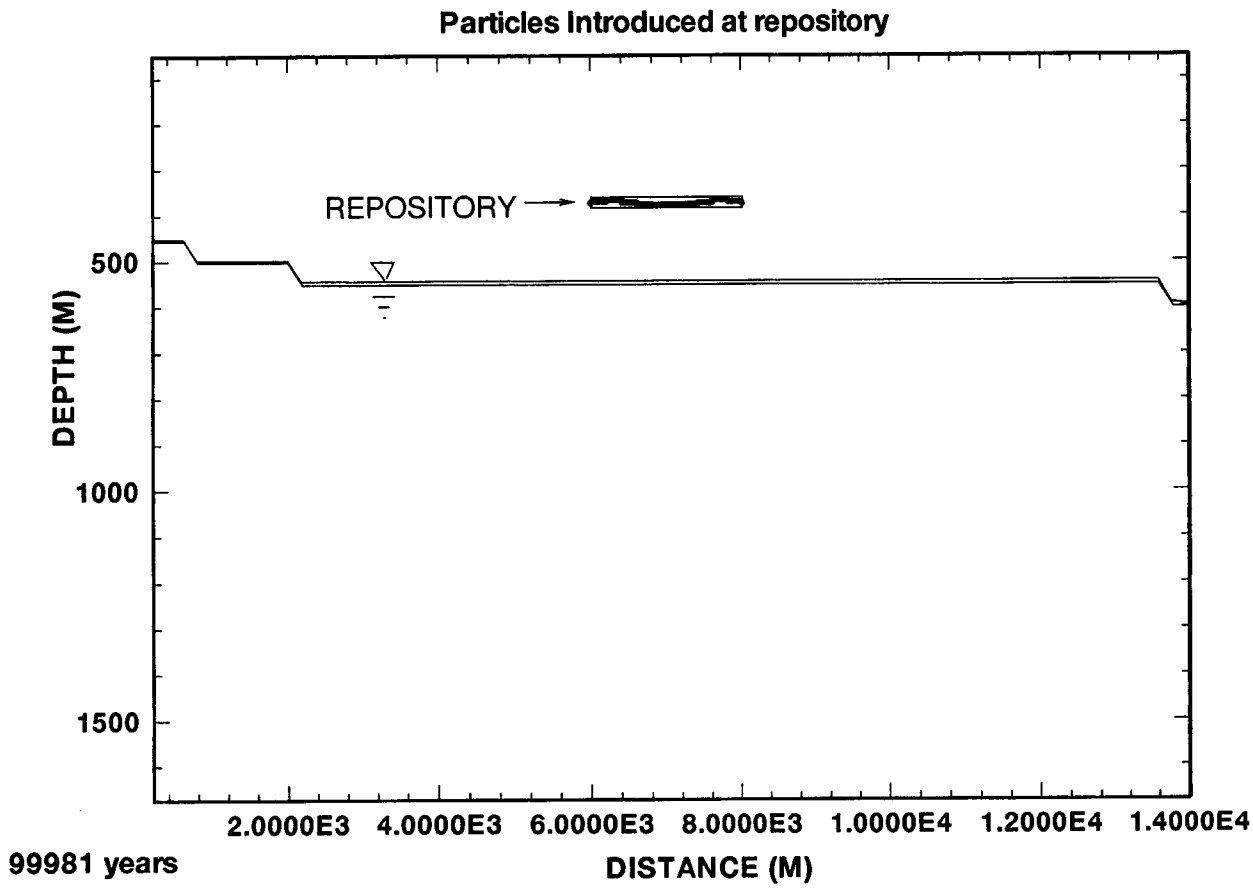

Figure 12. Location of 6,000 particles introduced at the repository and tracked for 100,000 yr

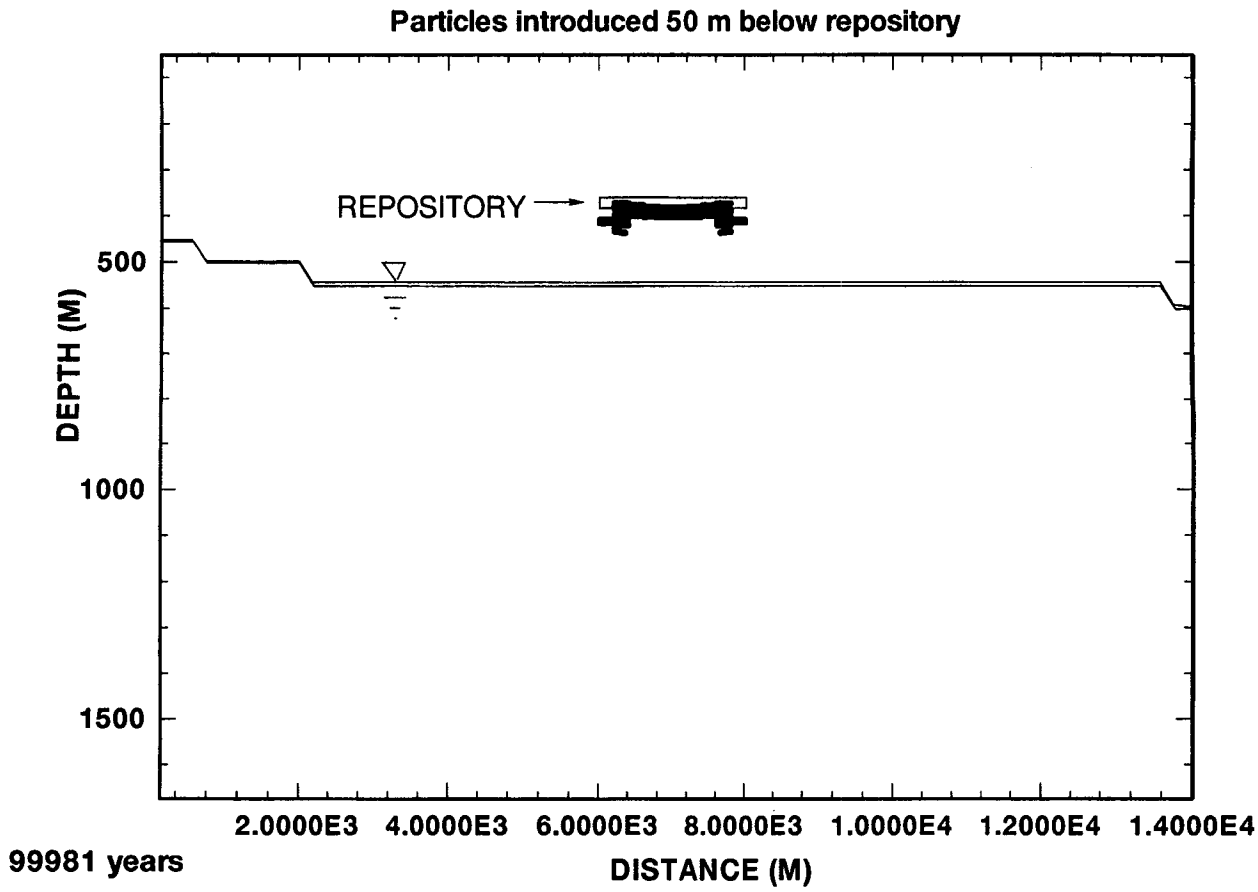

Figure 13. Location of 6,000 particles introduced at a horizon located 50 m immediately below the repository and tracked for 100,000 yr

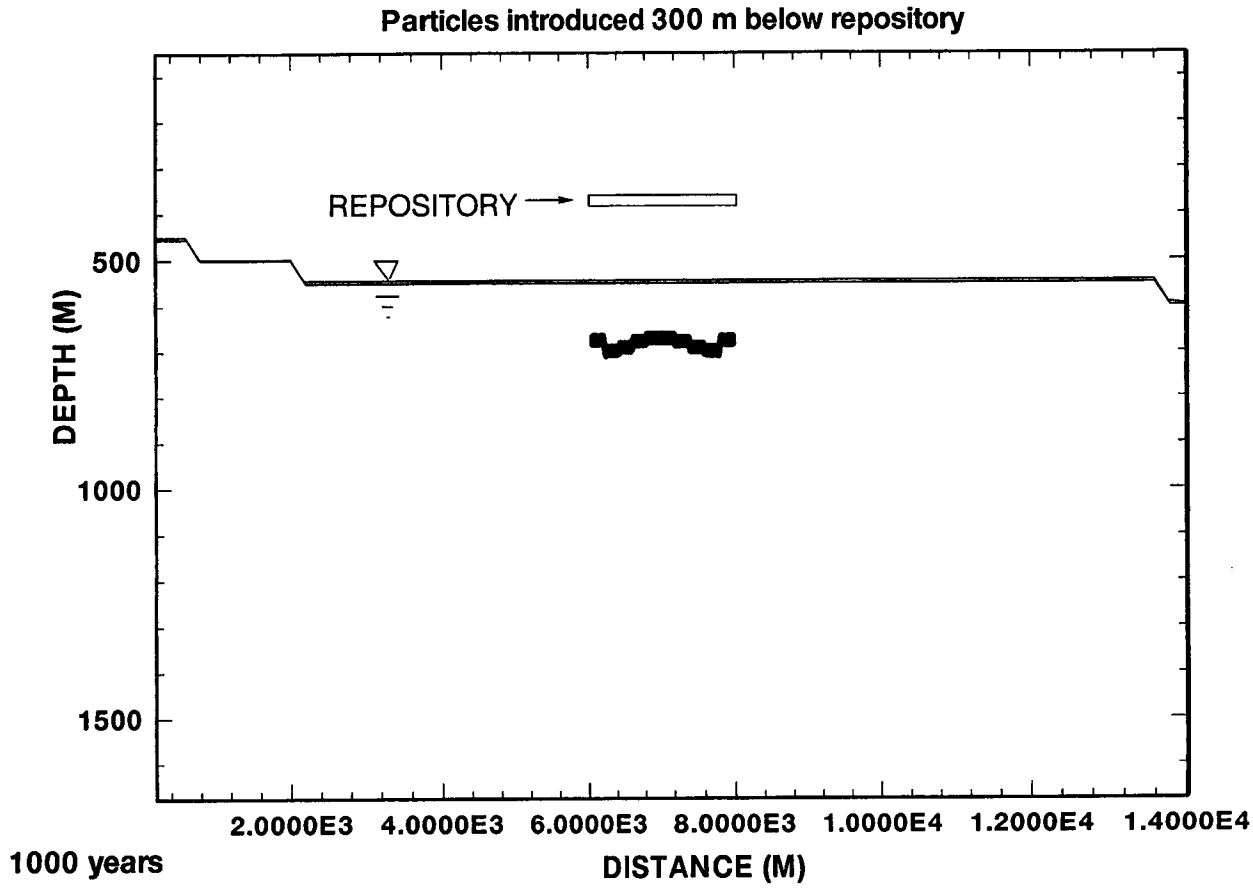

Figure 14. Location of 6,000 particles introduced at a horizon located 300 m immediately below the repository and tracked for 10,000 yr

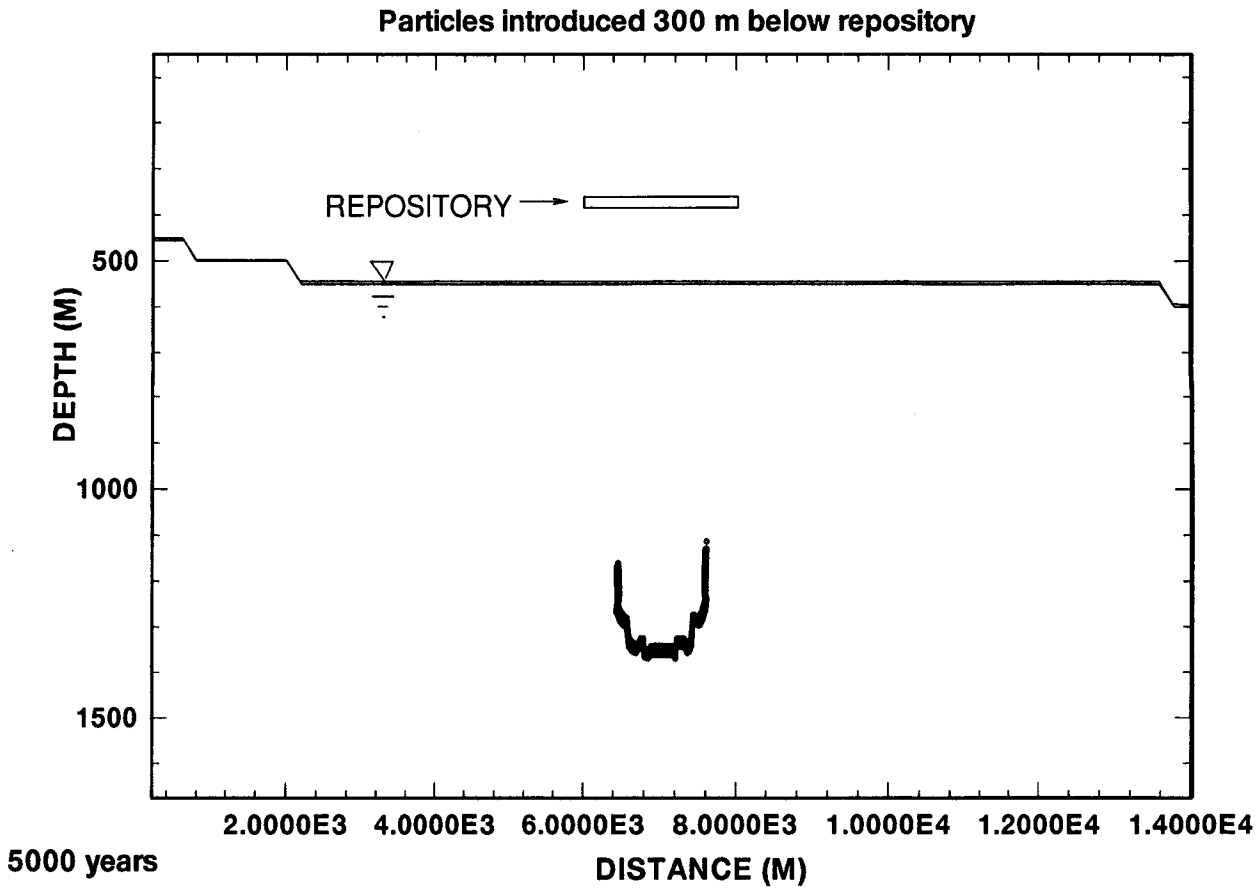

Figure 15. Location of 6,000 particles introduced at a horizon located 300 m immediately below the repository and tracked for 100,000 yr

common in nature, therefore, models which predict the formation of convection cells because these layers are absent may not be realistic. Consequently, the direction of flow in a more geologically realistic model could exhibit a horizontal component and the resulting flow regime would be less uniform than those predicted here. An important observation that can be made of the predictions of travel of particles introduced 300 m below the repository is that no particles reached the accessible environment compliance boundary within 5,000 yr, even for this extreme case of introducing the particles into the homogeneous, uniform saturated zone. This is partly attributable to the uniform movement of particles in the absence of any heterogeneous or complex geology. The inclusion of complicated geologic features, such as geologically reasonable pathways of higher permeability, could result in shorter particle travel times. This observation further supports the above discussed caveat that conclusions drawn from geologically simple models may not be conservative.

CONCLUSIONS

Analyses of flow and transport of particles in groundwater flow regimes for a saturated granite and a unsaturated/saturated tuff geologic setting have provided insight into the resolution of uncertainty associated with the GWTT rule, the performance measure for the geologic setting. The two sources of uncertainty are found in the terms "disturbed zone" and "fastest path of likely radionuclide travel". These two sets of analyses have evaluated separate aspects of the uncertainty. Since the repository is located in the unsaturated zone in the tuff geologic setting analyses, this set of analyses mostly provided insight into resolution of uncertainly associated with the disturbed zone. Similarly, analyses of particle travel from a repository located in saturated granite provided clarification in defining the fastest path of likely radionuclide travel. Together, analyses of the two geologic settings were instrumental in assessing the utility of a post-waste emplacement performance measure for the geologic setting.

Several conclusions regarding the appropriateness of performing GWTT calculations for post-waste emplacement conditions may be drawn from the results of the computational exercises conducted for the granite repository setting. It is more difficult to correctly define the regional flow regime for nonisothermal flow conditions than for isothermal flow conditions. The added difficulty posed by incorporating heat, even for this relatively simple saturated flow regime, is contrary to the goal of making GWTT a simple, and readily implementable measure of the geologic setting. The strong vertical gradients imposed by HLW generated thermal buoyancy effects cause most of the particles to travel vertically up, and those few particles that do reach the accessible environment do so by being conveyed to the surface. For the isothermal, conceptual model used in this study, it appears that most particles are transported downstream by the regional gradient where they are eventually captured by a fault or fracture zone. This is in contrast to the nonisothermal case in which particles are mostly transported vertically up due to thermal buoyancy. For the conceptual model used here, the dominant effects of thermal buoyancy, which drive the particles upward and away from the fracture zones, may prove to be beneficial insofar as the uncertainty in GWTT is markedly reduced.

By simulating multiple realizations of the flow regime in the granite setting, and by tracking 100 particles for each realization, tentative conclusions may be drawn regarding the feasibility of defining fastest path in a probabilistic sense. Statistics for the minimum travel times recorded for each of the 19 realizations performed for the nonisothermal case and each of the 20 realizations performed for the isothermal case are shown in Tables 3 and 4, respectively. The mean of the minimum travel times to compliance boundaries 1 through 4 for the nonisothermal case are remarkably close to those for the isothermal case. However, the shape of the distributions of the minimum travel times as shown by histograms in Figures

11 a-d, and 12 a-d are markedly different. For the three innermost compliance boundaries the mean of the minimum travel times significantly exceeds the median minimum travel times for both the isothermal and nonisothermal cases. This demonstrates that the distributions of minimum travel times for the first three compliance boundaries are positively skewed. If all minimum travel time distributions are positively skewed, the mean minimum travel time would not be an appropriate measure since it is not conservative. If the fastest path is to be interpreted in a probabilistic sense, it appears that a good rule could be written by specifying the median or 50th percentile of the minimum travel time distribution.

Several general observations on simulations of the tuff geologic setting can be made. The effect of the heat load is felt throughout the vertical extent of the model even after 50,000 yr into the simulation, although peak temperatures are greatly reduced by the end of the first 1,000 yr. From the temperature contours, water appears to flow downward from the repository toward the carbonate layer through the first 1,000 yr of the simulation then reverses and flows upward after 5,000 yr. This groundwater flow characteristic appears to be part of the convection cells that form in the saturated zone. The convection cells result in groundwater flow that is generally downward in the region up-gradient of the repository, and upward, down-gradient from the repository at all simulation times. The formation of model-scale convection cells has been attributed to the finite size of the model and the uniform, homogeneous nature of the medium. However, the generation of convection cells in a geologically real setting is questionable.

Tracking of particles introduced into the flow regime at a repository located in partially-saturated, uniform, homogeneous tuff results in unrealistic predictions of particle movement. The heat source establishes a flow regime in which liquid water is vaporized near the heat source and driven away from the repository by the vapor pressure gradient to a location where temperatures are lower and the vapor condenses. This fluid flow mechanism results in the formation of a liquid water capture zone encapsulating the heat source within which all liquid flow is toward the repository. This symmetric, uniform capture zone created by the heat source exists, in part, because the repository is located in a completely uniform, homogeneous medium. The inclusion of a persistent low or high permeability zone, such as a large fracture or a fault zone, may provide a conduit for downward liquid flow through the repository, particularly if heating near the repository is nonuniform. The downward flowing channel for liquid water could compromise the integrity of the liquid water capture zone encapsulating the repository, and allow particles to escape and move downward to the saturated zone. This scenario would be more realistic than the uniform, homogeneous model but would still fail to be truly representative of the geologic setting.

Simulations of groundwater flow for the unsaturated/saturated tuff geologic setting and the prediction of groundwater flow using the associated particle tracking scheme have provided evidence that strongly suggests that a post-waste emplacement performance measure does not resolve the uncertainties in 10 CFR 60.113(a)(2). The major evidence supporting this observation is the formation of a liquid water capture zone which encompasses a heat-generating repository located in partially-saturated rock. This formation of a capture zone is predicated on the premise that the medium is uniform and homogeneous and that no persistent flow features are included in the model. When a simple geologic model such as this is used to predict groundwater flow through use of tracked particles, all particles are captured by liquid water refluxing toward the heat source. Inclusion of heterogeneities and persistent linear flow features into the model could provide for a more geologically-realistic model. However, the additional computational burden imposed by increasing the degree of complexity may preclude the incorporation of nonisothermal processes into the transport mechanisms. Ultimately, one must choose either to incorporate nonisothermal components of flow, or to include a higher level of heterogeneity into the model, but not both. Inclusion of both attributes in the model is not computationally feasible. Since

exclusion of realistic features in the model produces unrealistic predictions of groundwater travel pathways, a realistic geologic model probably precludes the incorporation of nonisothermal transport processes. For this reason alone, a post-waste emplacement performance measure for the geologic setting should probably be abandoned. However, it must be stressed that this conclusion has been drawn from a limited number of computations. Computations incorporating additional features, such as infiltration at the upper boundary, and a wider range of possible boundary conditions and property values would provide additional insight into this investigation. However, future efforts may be better spent pursing other, more promising, resolution methodologies to reduce uncertainty in the GS performance measure, than a post-waste emplacement measure.

RECOMMENDATIONS

The analyses conducted here to reduce uncertainty in the GS performance measure have led to a refinement in the options available for resolution of the GWTT rule. Conclusions from this most recent set of analyses suggest that a post-waste emplacement performance measure has enough problems to make it unusable. Moreover, results from these analyses have led to the identification and clarification of which resolution methodologies hold promise and which, in addition to those predicated on post-waste emplacement, should be abandoned. Following is a refined list of options which continue to provide potential resolution to uncertainty reduction in the GWTT rule. Two of the options would require a rulemaking while the other two could be resolved with a Technical Position (TP). All four options are pre-waste emplacement.

- Option I. Change the definition of "disturbed zone" in 10 CFR 60.2. The revised wording would be "*Disturbed zone* means that portion of the controlled area the physical or chemical properties of which have changed as a result of underground facility construction or as a result of heat generated by the emplaced radioactive wastes such that the resultant change intrinsic permeability and porosity may have a significant effect on the performance of the geologic repository." By changing the present wording "properties" to "intrinsic permeability and porosity," ambiguity associated with defining the extent of the disturbed zone could be reduced. The extent of the disturbed zone would then be defined as the area encompassing the media that experiences a performance-affecting change in intrinsic permeability and porosity. Changes in fluid properties (i.e., buoyancy resulting from fluid density changes) would not be incorporated into the GS performance measure calculations. This option would require a rulemaking.

- Option II. Remove the term "disturbed zone" from 10 CFR 60.113(a)(2) and increase GWTT to some value greater than 1,000 yr to account for the fact that a longer pathway is used in the calculation. Ambiguity associated with defining the extent of the disturbed zone is removed. This option would require a rulemaking.

- Option III. Leave the current language in 10 CFR 60.113(a)(2) intact but provide guidance to DOE using a TP. The TP would clarify to DOE what would be acceptable to NRC in terms of "fastest path of likely radionuclide travel" and "disturbed zone." No rulemaking would be required for this option.

- Option IV. No guidance would be provided to DOE nor would there be a rulemaking to resolve potential uncertainties in 10 CFR 60.113(a)(2). This option would abandon the current pro-active posture maintained by the NRC.

The resolution of uncertainty associated with defining the extent of the "disturbed zone" is addressed in Options I, II and III. However, the utility of either of these resolution methodologies is yet to be demonstrated. Assessment of Options I and III requires similar exercises to determine their potential utility to reduce uncertainty in the GS performance measure. First, a viable definition for the extent of the disturbed zone has to be identified. It is anticipated that this exercise will be pursued along the lines described in Option I, that is, the extent of the disturbed zone will be limited to media that experience negative performance affecting changes in media properties (e.g., increases in porosity or permeability), but will not depend on changes in fluid properties. Second, groundwater flow through the subsurface will be isothermal but will accommodate persistent conduits or flow barriers, and media heterogeneities. Groundwater flow will be determined for pathways initiated at the disturbed zone boundary and terminated at the accessible boundary.

Demonstration and assessment of Option II will consist of only part of the assessment methodology identified in Options I and III, that is, the prediction of the "fastest path of likely radionuclide travel" isothermal groundwater flow through heterogeneous media. The concept of a disturbed zone will be abandoned and the travel time will be increased. Resolution of the GS performance measure through either Options I or III will become more attractive and the impetus to choose Option II will be decreased should resolution of uncertainty associated with the "disturbed zone" prove to be acceptable.

Uncertainty remains in defining the "fastest path of likely radionuclide travel" in the first three of these options. Resolution of uncertainty in the term "fastest path" is independent of a decision to select either a pre- or post-waste emplacement performance measure. As such conclusions from analyses of GWTT for the granite geologic setting have provided insight toward resolving this uncertainty. These conclusions indicate that distributions of particle arrival times are capable of providing a quantifiable measure of "fastest path." Personal communication with J. Pohle (1994) has identified a potential methodology to determine the "fastest path" in context of arrival time distributions. In this approach, multiple stochastic realizations would each provide a distribution of particle arrival times at the compliance boundary. Only the arrival of the first particle from each realization would be retained for analysis. The mean or median of the distribution of first arrivals could then be the value assigned to the "fastest path of likely radionuclide travel." Resolution of this uncertainty, however, is not final. Additional clarification is required to identify which property or characteristic of the arrival distributions constitutes the "fastest path."

Finally, Option IV could be selected if it appears that approaches taken by DOE are acceptable and do not require additional uncertainty reduction or guidance. There is a risk contained in Option IV that DOE could modify their methodology or interpretations in ways unacceptable to NRC, particularly if such changes occur late in the licensing process.

The conclusion that the retention of all particles within the capture zone encapsulating the repository in unsaturated media is evidence that GWTT's are very large (i.e., greater than 100,000 yr) and therefore that a post-waste emplacement performance measure is a valid measure of the performance of the geologic setting is incorrect. The models tested in these analyses are too limited, especially in terms of the degree of geologic complexity that has been included, to support the contention that the models represent an actual physical setting. Models that are more geologically realistic could predict particle movement

significantly different than that predicted here, particularly in the tuff geologic setting which contains the least complicated geology. However, due to limitations in computational capabilities, model predictions for two-phase flow cannot incorporate an adequate level of geologic detail to insure the predictions are representative of a candidate site. This limitation is sufficiently significant at the present that improvements in computation capabilities for the foreseeable future will still not provide the means to predict two-phase flow for repository-scale models. For these reasons, a post-waste emplacement performance measure for the geologic settings is dismissed as an attractive option to resolving uncertainty in the GWTT rule.

REFERENCES

Bagtzoglou, A.C., and M.A. Muller. 1994. *Stochastic Analysis of Large-Scale Unsaturated Flow and Transport in Layered, Heterogeneous Media.* CNWRA 94-012. San Antonio, TX: Center for Nuclear Waste Regulatory Analyses.

Brandshaug, T. 1991. *A Thermochemical Far-Field Model of Yucca Mountain.* SAND85-7101. Albuquerque, NM: Sandia National Laboratory.

Buscheck, T.A., and J.J. Nitao. 1992. The impact of thermal loading on repository performance at Yucca Mountain. *Proceedings of the Third High-Level Waste Management Conference International Conference*: Las Vegas, NV.

Freeze, R.A., and J.A. Cherry. 1979. *Groundwater*. Edgewood Cliffs, NJ: Prentice Hall, Inc.

Guzowski, R.V., F.B. Nimick, M.D. Siegel, and N.C. Finley. 1983. *Repository Site Data for Tuff: Yucca Mountain, Nevada*. NUREG/CR-2937. Washington, DC: Nuclear Regulatory Commission.

Inman, R.L., and M.J. Shortencarier. 1984. *A FORTRAN Program and User's Guide for the Generation of Latin Hypercube and Random Samples for Use With Computer Models*. SAND83-2365. Albuquerque, NM: Sandia National Laboratories.

Isherwood, D. 1981. *Geoscience Data Base for Modeling a Nuclear Waste Repository*. NUREG/CR-0912, Volumes 1 and 2. Washington, DC: U.S. Nuclear Regulatory Commission.

Klavetter, E.A., and R.R. Peters. 1986. *Estimation of Hydrologic Properties of an Unsaturated, Fractured Rock Mass*. SAND84-2642. Albuquerque, NM: Sandia National Laboratories.

Mercer, J.W., S.D. Thomas, and B. Ross. 1982. *Parameters and Variables Appearing in Repository Siting Models*. NUREG/CR-3066. Washington, DC: U.S. Nuclear Regulatory Commission.

Nitao, J.J. 1988. *Numerical Modeling of the Thermal and Hydrological Environment Around a Nuclear Waste Package Using the Equivalent Continuum Approximation: Horizontal Emplacement*. UCID-21444. Livermore, CA: Lawrence Livermore National Laboratory.

Nitao, J.J. 1989. *V-TOUGH. An Enhanced Version of the TOUGH Code for the Thermal and Hydrologic Simulation of Large-Scale Problems in Nuclear Waste Isolation.* UCID-21954. Livermore, CA: Lawrence Livermore Laboratory.

Pruess, K. 1987. *TOUGH. User's Guide.* NUREG/CR-4645. Washington, DC: Nuclear Regulatory Commission.

Rice, G., R.T. Green, and J.A. Pohle. 1993. *Reduction in Uncertainty in the Geologic Setting Performance Measure, 10 CFR 60.113(a)(2): Conceptual Models and Databases.* CNWRA. San Antonio, TX: Center for Nuclear Waste Regulatory Analyses.

Tien, P.-L., M.D. Siegel, C.D. Updegraff, K.K. Wahi, and R.V. Guzowski. 1985. *Repository Site Data Report for Unsaturated Tuff, Yucca Mountain, Nevada.* NUREG/CR-4110. Washington, DC: U.S. Nuclear Regulatory Commission.

U.S. Department of Energy. 1988. *Site Characterization Plan.* Washington, DC: U.S. Department of Energy.

U.S. Nuclear Regulatory Commission. 1993. *Phase 2 Demonstration of the NRC's Capability to Conduct a Performance Assessment for a Level Waste Repository.* NUREG-1464. Washington, DC: U.S. Nuclear Regulatory Commission. In preparation.

Weast, R.C., ed. 1981. *CRC Handbook of Chemistry and Physics, 60th Edition.* Boca Raton, FL: CRC Press, Inc.

19/30

APPENDIX A

Granite Geologic Setting—Conceptual Model and Parameter Values

Table A-1. Summary of parameter values for granite geologic setting conceptual model

Property	Value
Granitic Batholith	
Thickness	> 5 km
Hydraulic conductivity - horizontal	1.0 E-9 m/s
Hydraulic conductivity - vertical	1.0 E-10 m/s
Effective porosity	1%
In situ hydraulic gradient - horizontal	0.01%
Fault Zone	
Thickness	2 m
Hydraulic conductivity	1.0 E-6 m/s
Effective porosity	10%
Repository	
Thickness	10 m
Hydraulic conductivity - horizontal	1.0 E-8 m/s
Hydraulic conductivity - vertical	1.0 E-8 m/s
Effective porosity	10%
All Units	
In situ geothermal gradient	2.5 C/100 m
Thermal conductivity	3.2 W/m-C
Specific heat	990 J/kg-C
Boundary Conditions	
Point A	
Hydraulic head*	4050 m H_2O (3.9705 E+7 Pa)
Temperature	45.0 C
Point B	
Hydraulic head*	4000 m H_2O (3.9215 E+7 Pa)
Temperature	45.0 C
Point C	

Table A-1. Summary of parameter values for granite geologic setting conceptual model (Cont'd)

Property	Value
Hydraulic head*	4050 m H_2O (3.9705 E+7 Pa)
Temperature	47.5 C
Point D	
Hydraulic head*	4000 m H_2O (3.9215 E+7 Pa)
Temperature	47.5 C
*Modified from original report by Rice et al., 1993.	

Table A-2. Parameter value ranges and document sources for granite geologic setting. Document sources are: (1) Isherwood (1981), and (2) Mercer et al. (1982).

Property	Range	Document Source	Representative Value	Document Source
Hydraulic conductivity - matrix	8.6 E-13 - 3.8 E-9 m/s	1 - V2, p 304	1.0 E-11 m/s	1 - V2, p 315
Hydraulic conductivity - fractured	2.0 E-11—4.6 E-5 m/s	1 - V2, p 304	1.0 E-9 m/s	1 - V2, p 315
Porosity	0.07 - 3%	1 - V2, p 304	1%	1 - V2, p 304
Density	2520 - 2810 kg/m^3	2, p 127	2670 kg/m^3	2, p 127
Dispersivity - longitudinal (fractured schist-gneiss)	—	—	134.1 m	1 - V1, p 212
Thermal conductivity	1.51 - 4.48 W/m-C	1 - V2, p 258	3.25 W/m-C	2 - p 118
Specific heat	804 - 1009 J/kg-C	2 - p 125, 1 - V2, p 266	990 J/kg-C	1 - V2, p 264
Thermal diffusivity	—	—	1.47 E-6 m^2/s	1 - V2, p 296

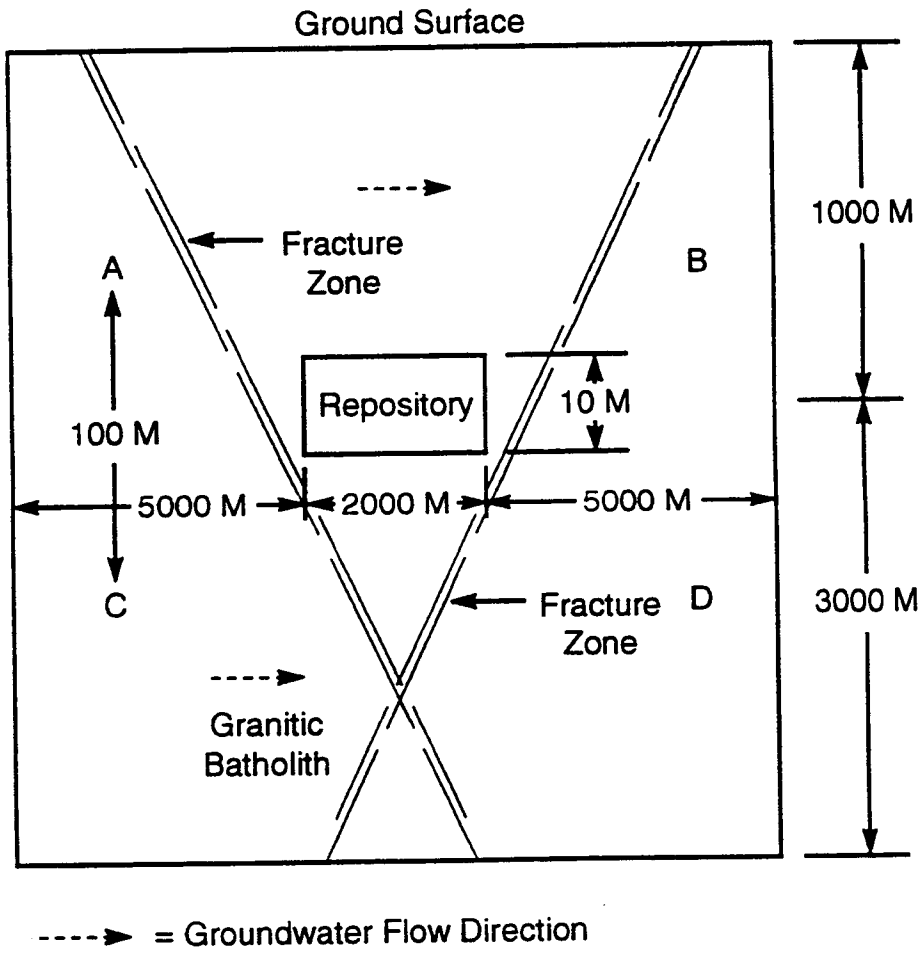

Figure A-1. Granite geologic setting conceptual model

21/30

APPENDIX B

Groundwater Travel Time Histograms for the Granite Geologic Setting

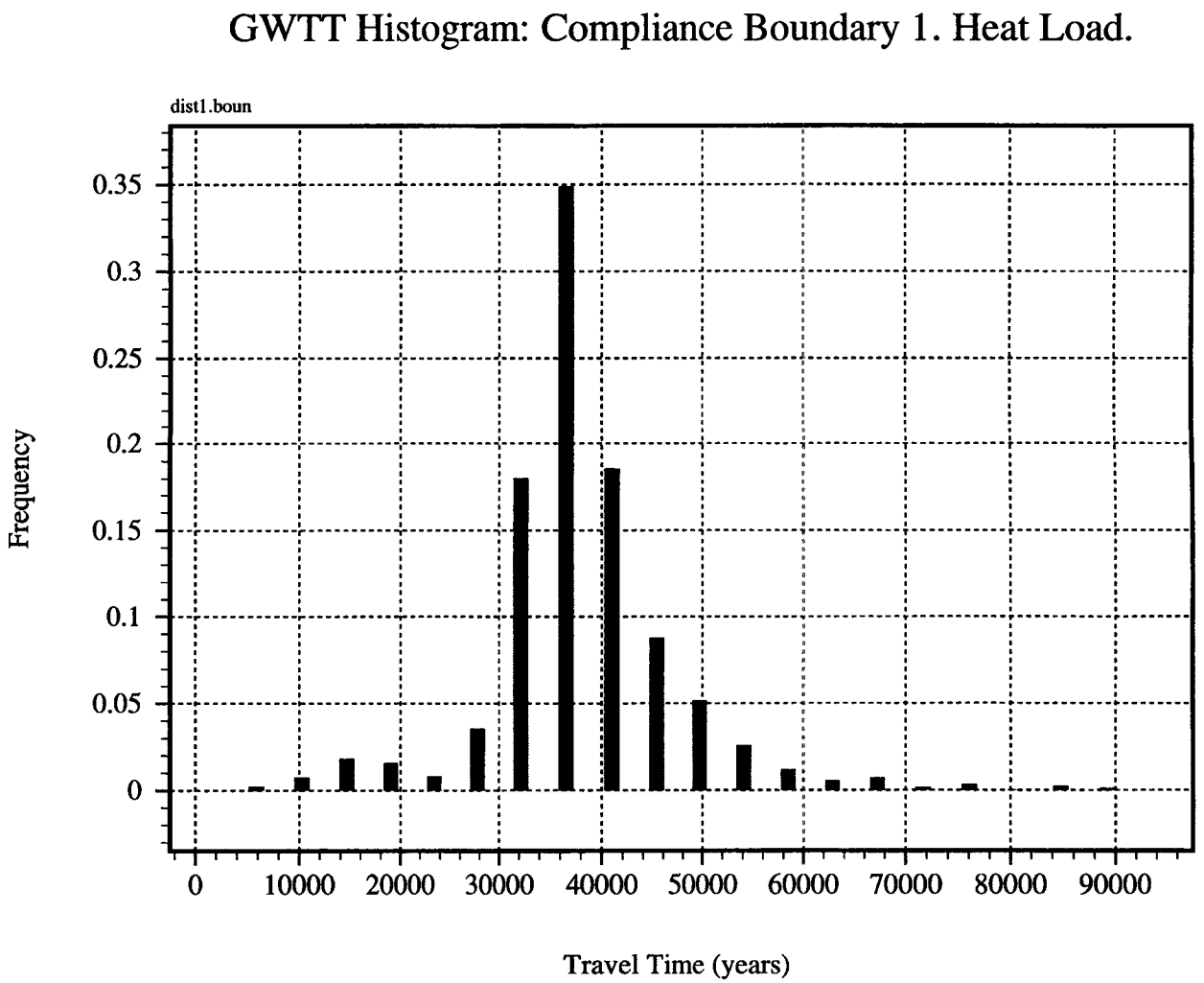

Figure B-1. Distribution of particle travel times to compliance boundary 1. Nonsiothermal case.

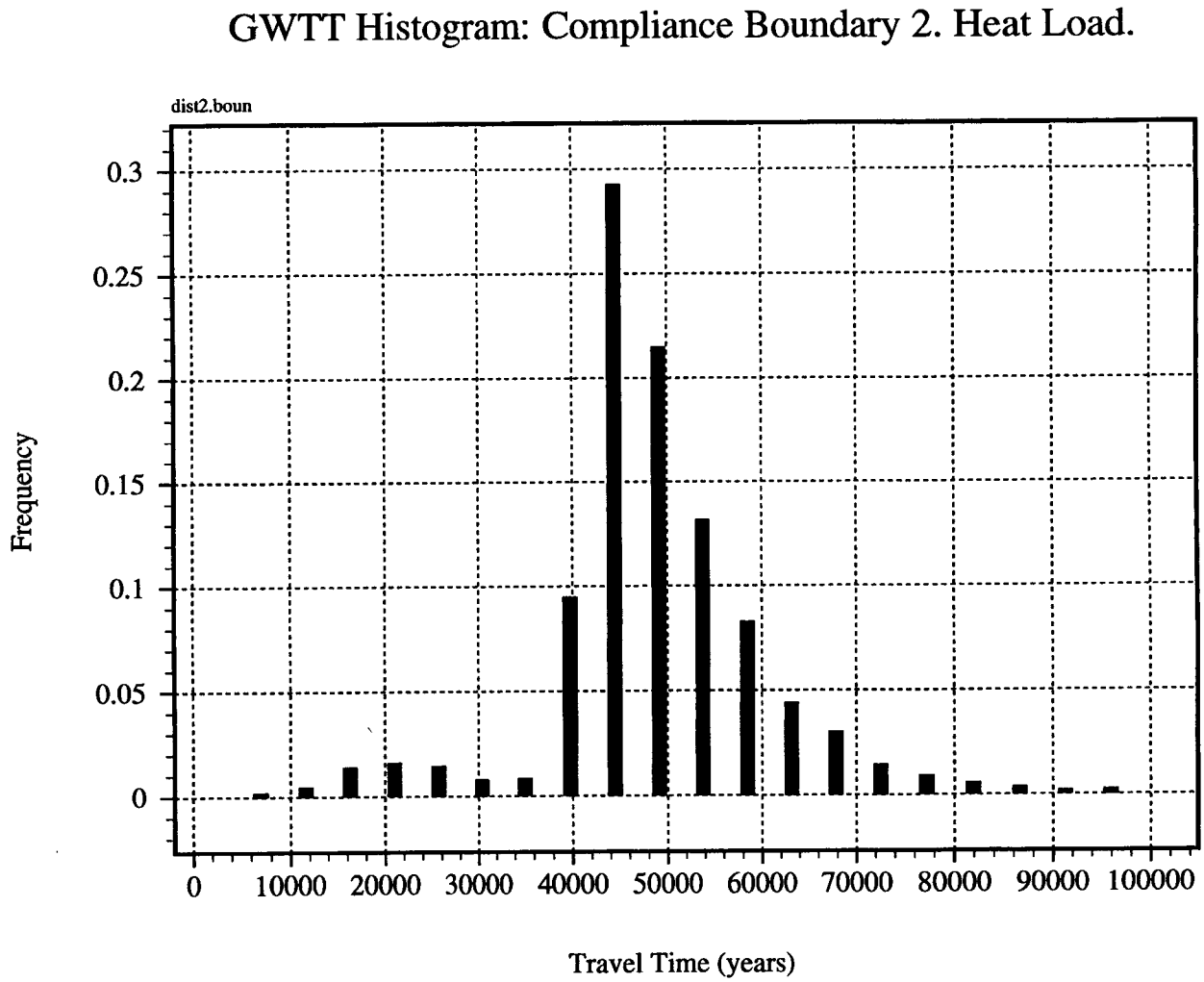

Figure B-2. Distribution of particle travel times to compliance boundary 2. Nonsiothermal case.

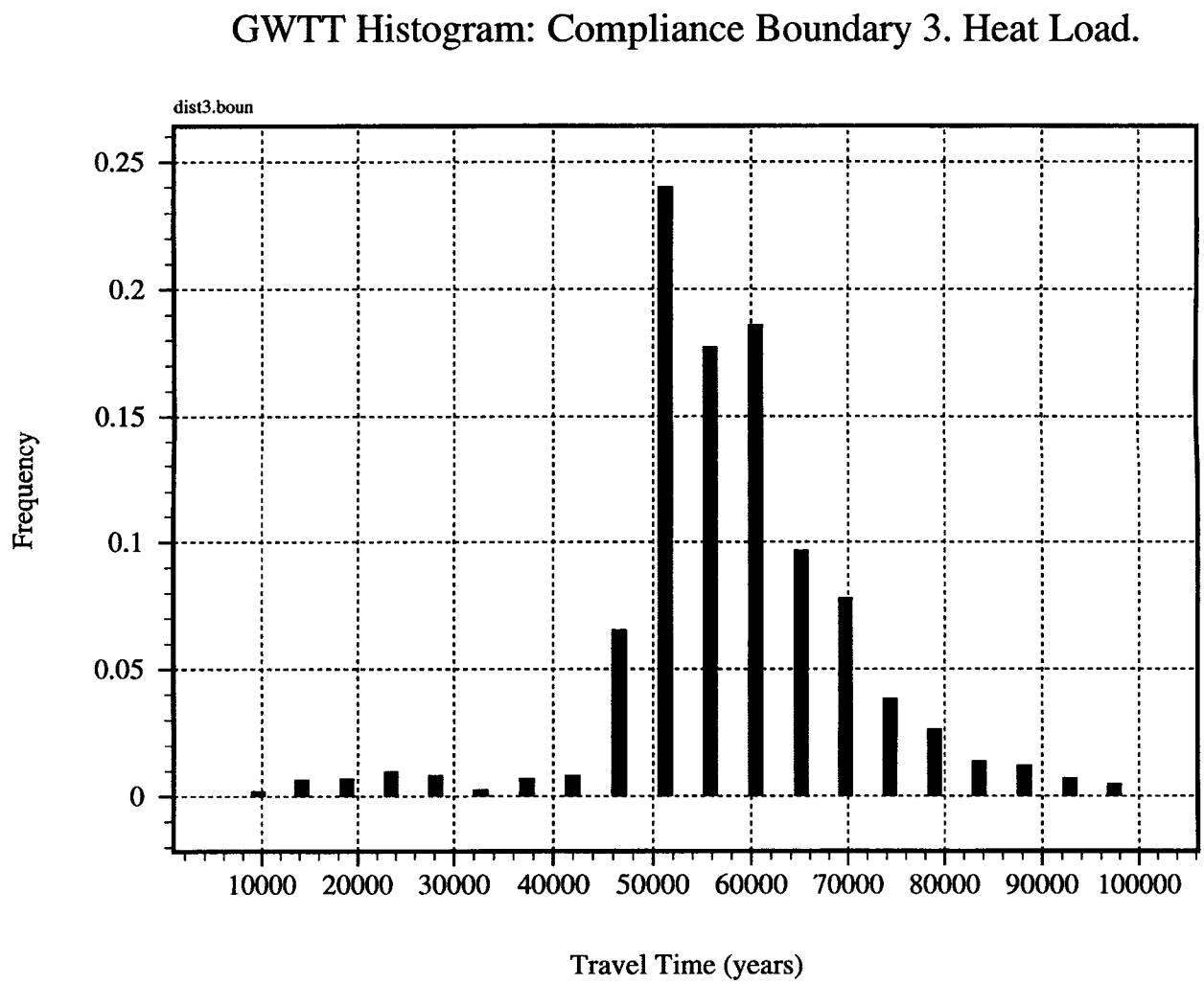

Figure B-3. Distribution of particle travel times to compliance boundary 3. Nonsiothermal case.

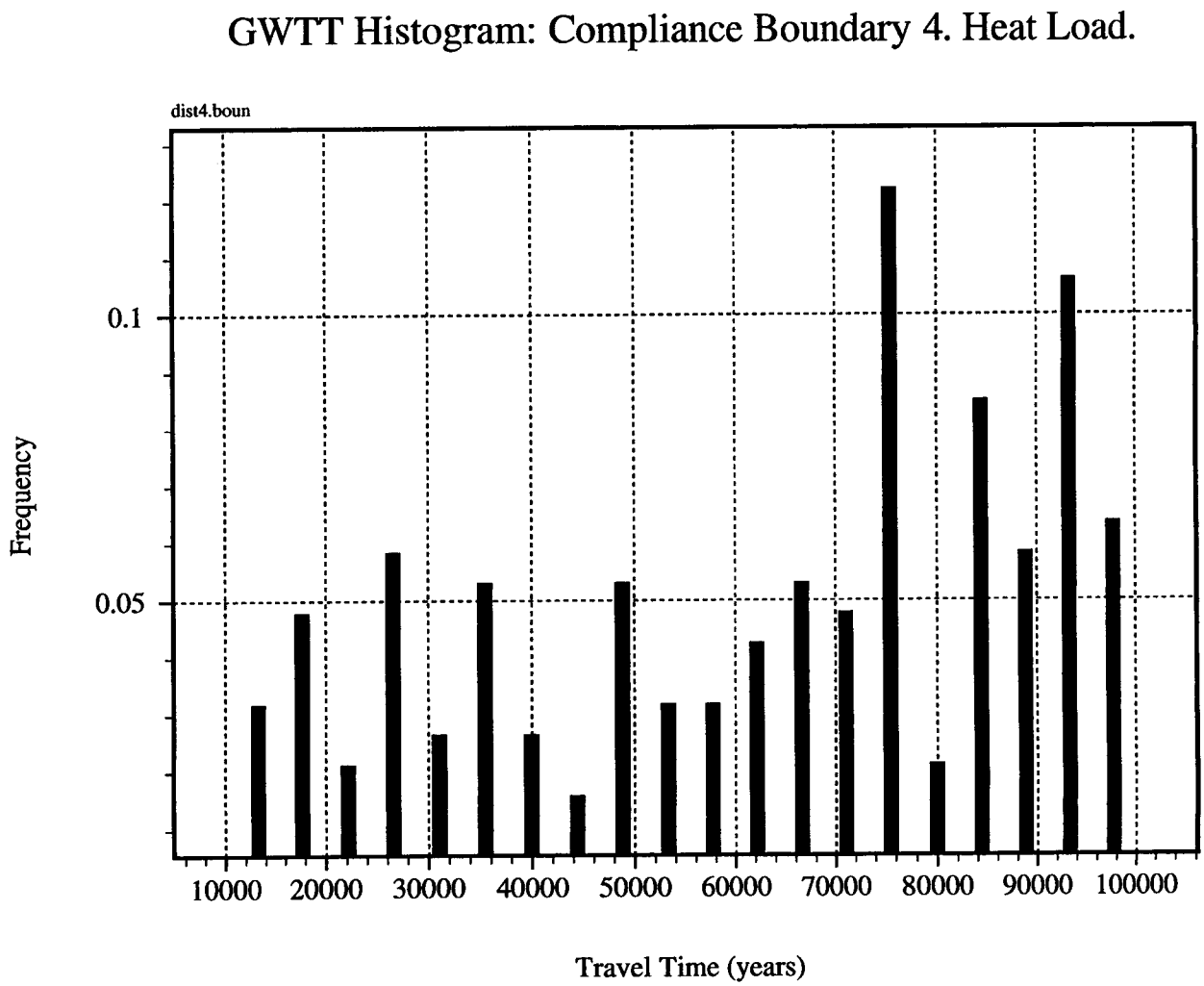

Figure B-4. Distribution of particle travel times to compliance boundary 4. Nonsiothermal case.

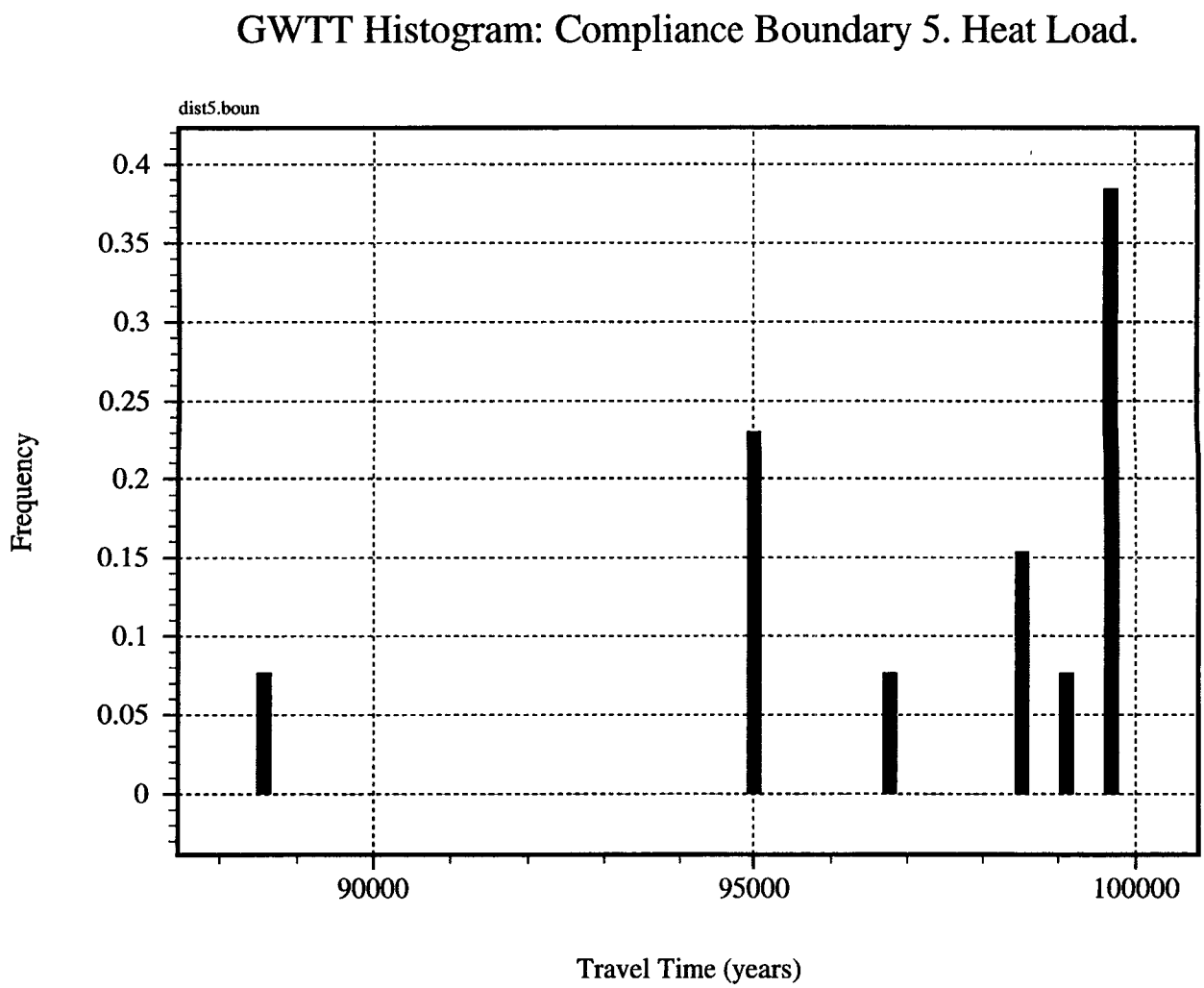

Figure B-5. Distribution of particle travel times to compliance boundary 5. Nonisothermal case.

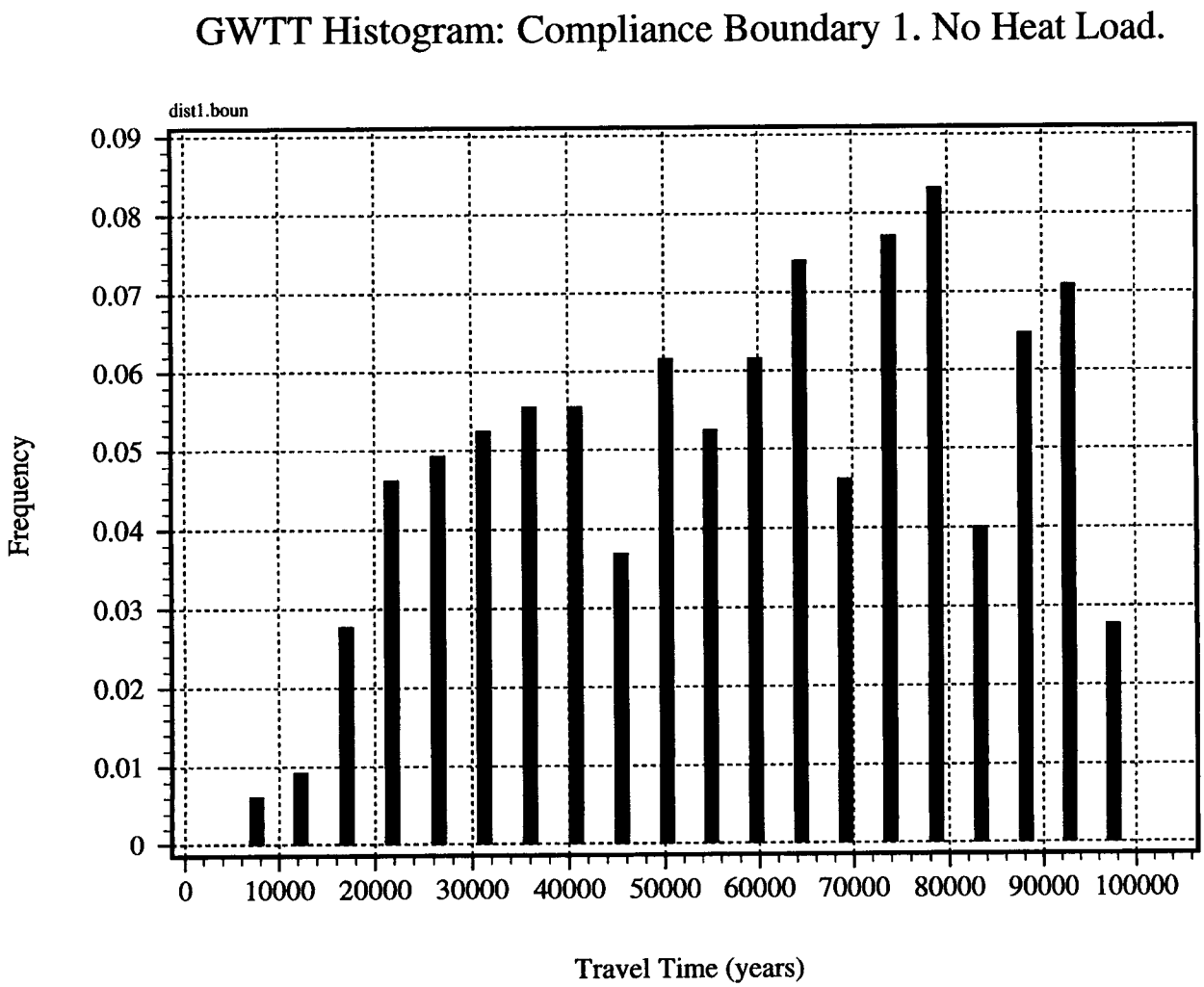

Figure B-6. Distribution of particle travel times to compliance boundary 1. Isothermal case.

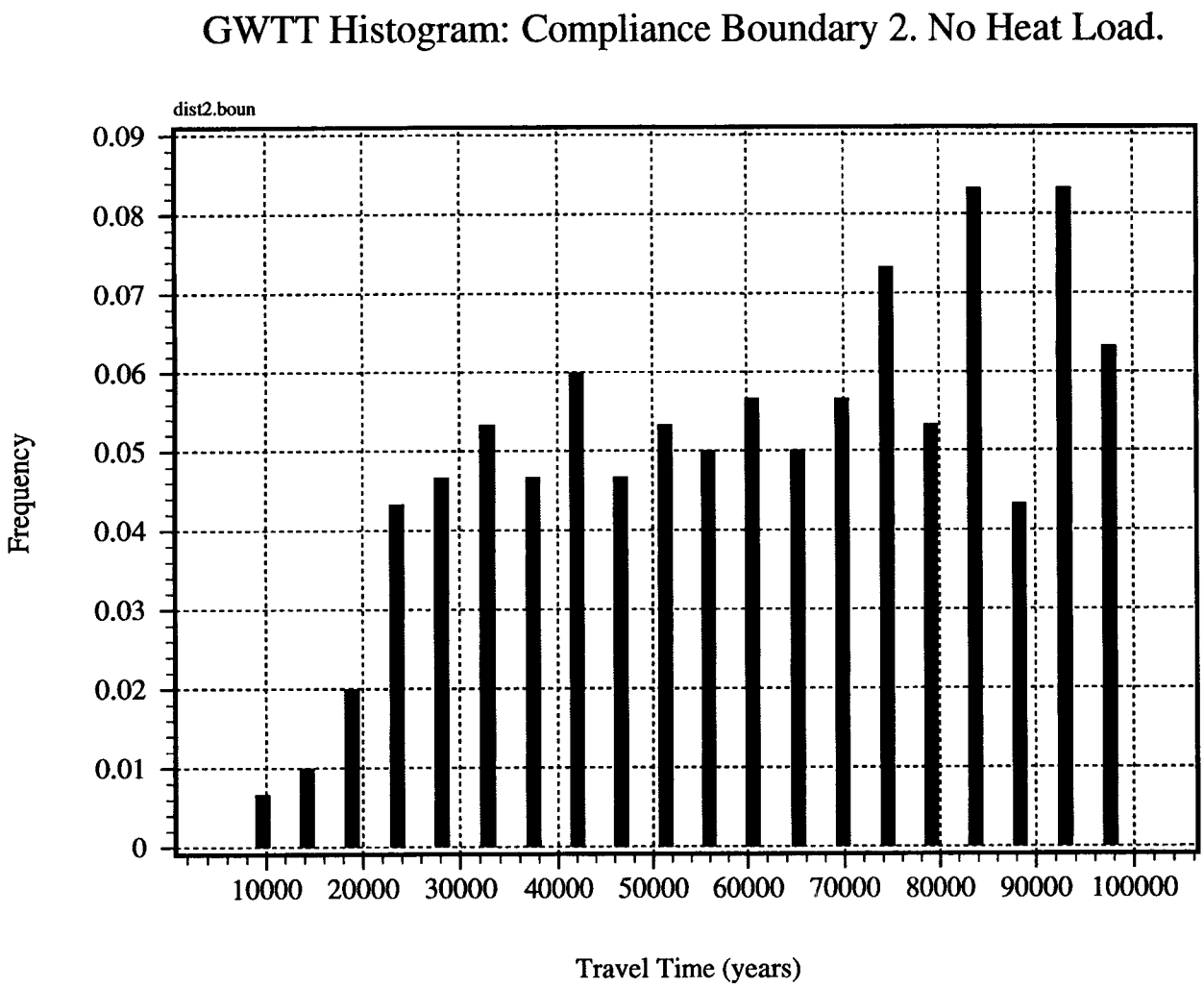

Figure B-7. Distribution of particle travel times to compliance boundary 2. Isothermal case.

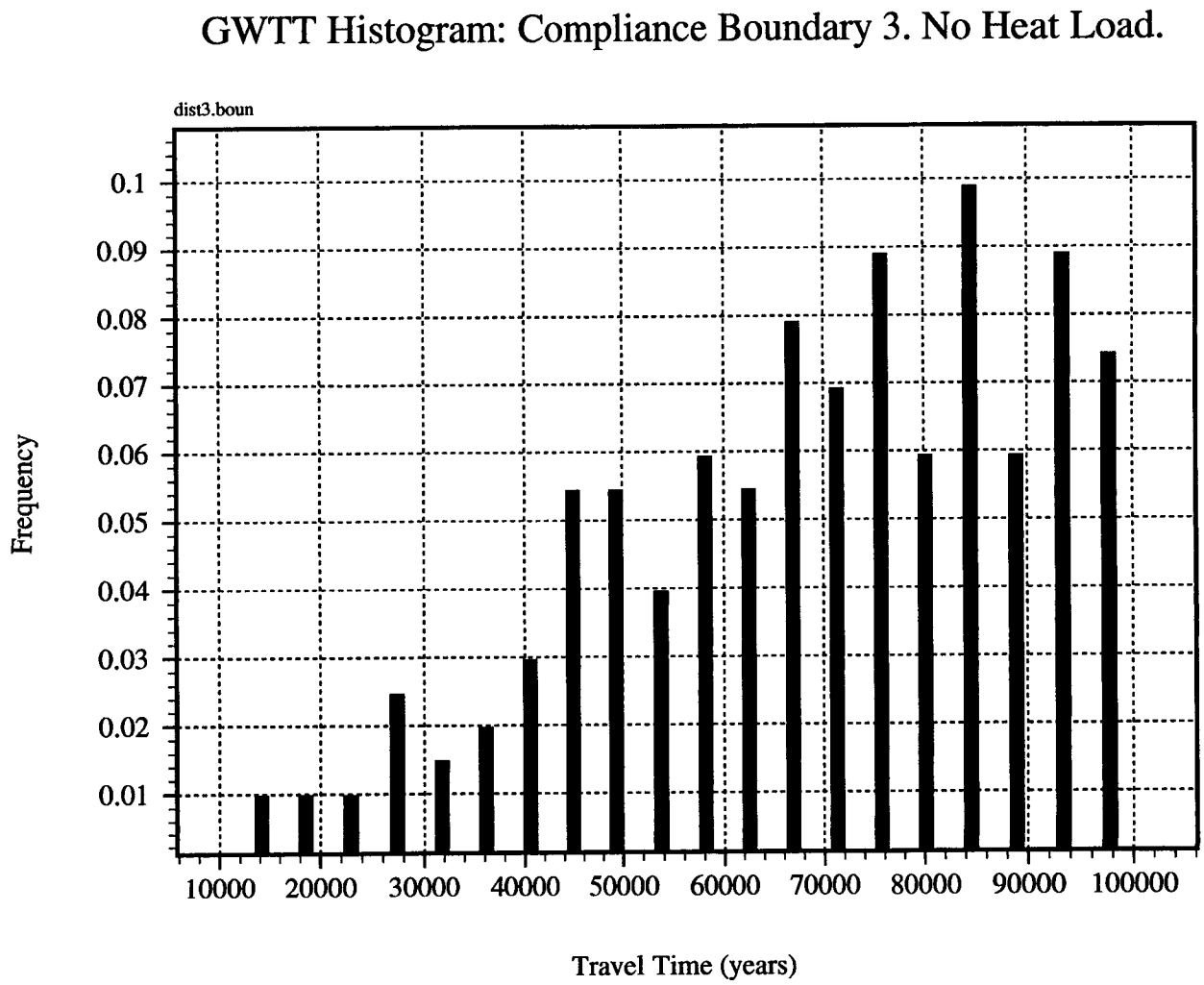

Figure B-8. Distribution of particle travel times to compliance boundary 3. Isothermal case.

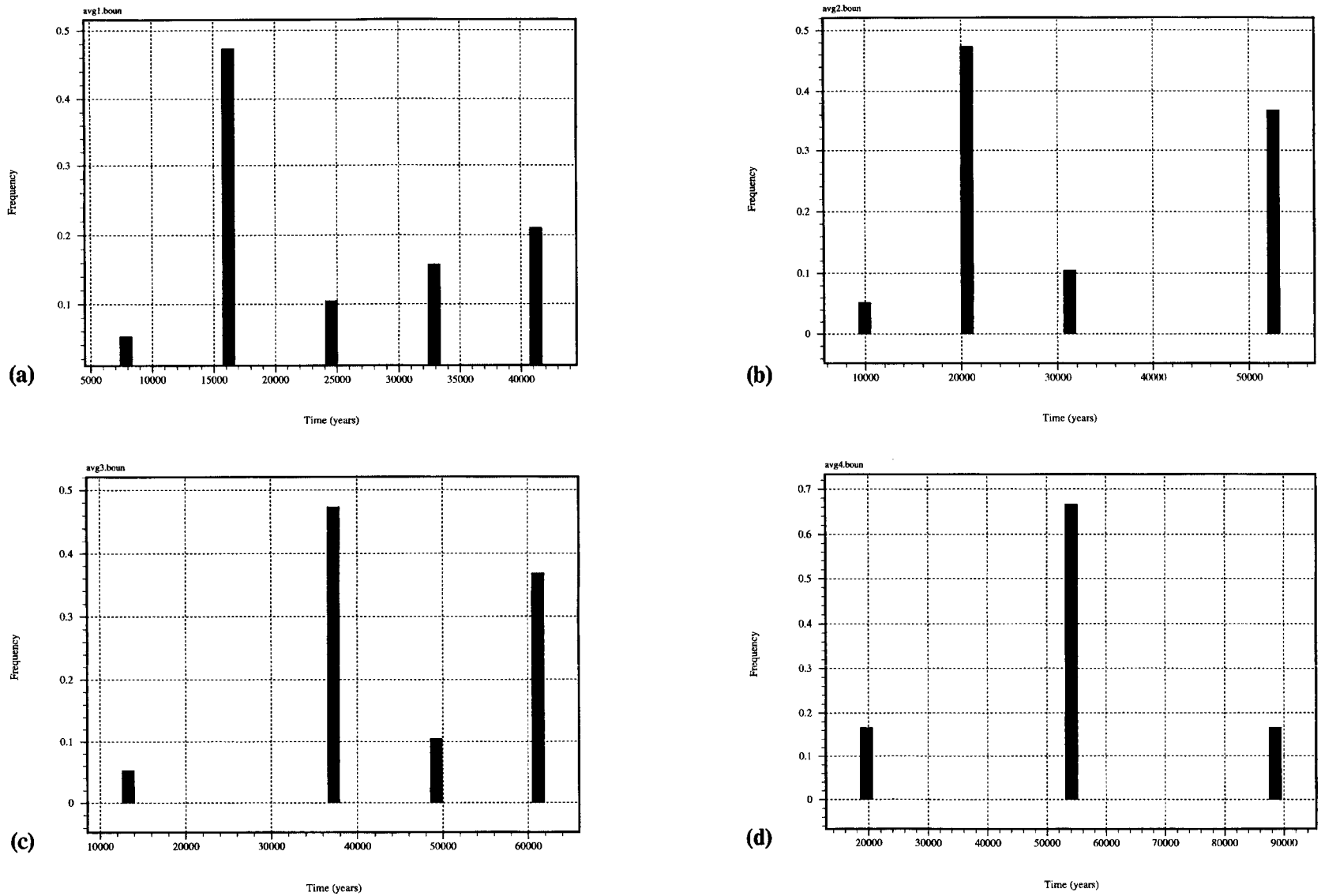

Figure B-9. Distribution of minimum particle travel times for the nonisothermal case: (a) compliance boundary 1, (b) compliance boundary 2, (c) compliance boundary 3, and (d) compliance boundary 4

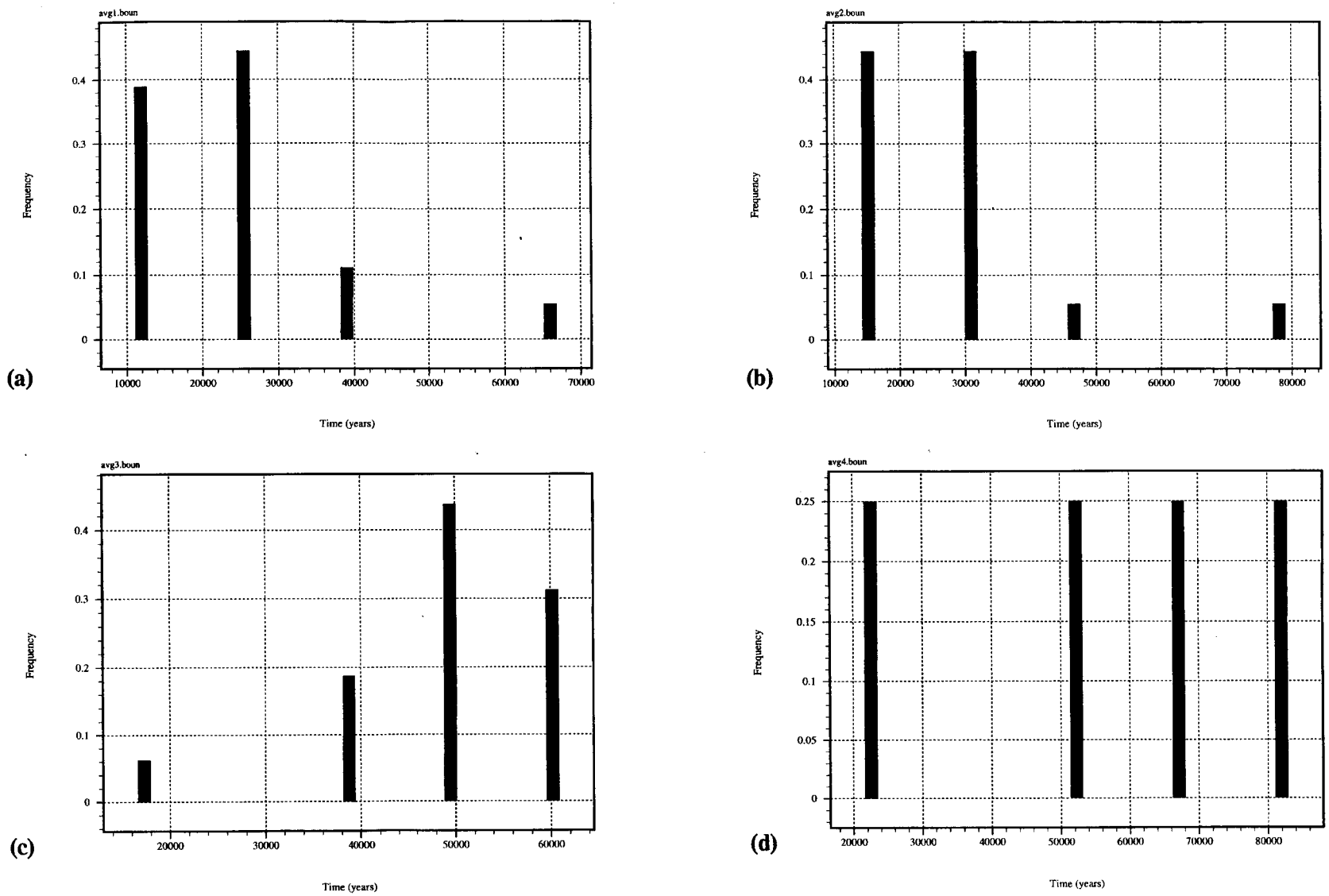

Figure B-10. Distribution of minimum particle travel times for the isothermal case: (a) compliance boundary 1, (b) compliance boundary 2, (c) compliance boundary 3, and (d) compliance boundary 4

26/30

27/30

APPENDIX C

Tuff Geologic Setting—Conceptual Model and Parameter Values

Table C-1. Summary of parameter values for the tuff geologic setting conceptual model

Property	Value
Unsaturated Tuff	
Thickness	550 m
Hydraulic conductivity - matrix	6.3 E-11 m/s
Hydraulic conductivity - fracture	1.5 E-9 m/s
Effective porosity - matrix	5%
Effective porosity - fracture	0.004%
van Genuchten α - matrix	0.006/m
van Genuchten α - fracture	1.3/m
van Genuchten β - matrix	1.8
van Genuchten β - fracture	4.2
In situ hydraulic gradient - vertical	1%
Thermal conductivity	1.7 W/m-C
Specific heat	1150 J/kg-C
Saturated Tuff	
Thickness	1000 m
Hydraulic conductivity - matrix	6.3 E-11 m/s
Hydraulic conductivity - fracture	1.5 E-9 m/s
Effective porosity - matrix	5%
Effective porosity - fracture	0.004%
In situ hydraulic gradient - vertical	1%
Thermal conductivity	1.7 W/m-C
Specific heat	1150 J/kg-C
Limestone Aquifer	
Thickness	50 m
Hydraulic conductivity	1 E-6 m/s
Effective porosity	5%
In situ hydraulic gradient - horizontal	0.005%

Table C-1. Summary of parameter values for the tuff geologic setting conceptual model (Cont'd)

Property	Value
Thermal conductivity	3.6 W/m-C
Specific heat	904 J/kg-C
Repository	
Thickness	10 m
Hydraulic conductivity - horizontal	1.0 E-8 m/s
Hydraulic conductivity - vertical	1.0 E-8 m/s
Effective porosity	10%
Thermal conductivity	1.7 W/m-C
Specific heat	1150 J/kg-C
All Units	
Geothermal gradient	2.5 C/100 m
Boundary Conditions	
Point A	
Elevation	1500 m H_2O (1.4706 E+7 Pa)
Pressure head	−30.6 m H_2O (3 E+5 Pa)
Total head	1469.4 m H_2O (1.4406 E+7 Pa)
Saturation - matrix	80%
Saturation - fracture	80%
Temperature	10.0 C
Point B	
Elevation	1475 m H_2O (1.4706 E+7 Pa)
Pressure head	−30.6 m H_2O (3 E+5 Pa)
Total head	1444.4 m H_2O (1.4161 E+7 Pa)
Saturation - matrix	80%
Saturation - fracture	80%
Temperature	10.0 C
Point C (above water table)	

Table C-1. Summary of parameter values for the tuff geologic setting conceptual model (Cont'd)

Property	Value
Elevation	950 m H_2O (9.3136 E+6 Pa)
Pressure head	−30.6 m H_2O (3 E+5 Pa)
Total head	919.4 m H_2O (9.0136 E+6 Pa)
Saturation – matrix	80%
Saturation – fracture	80%
Temperature	23.8 C
Point C (below water table)	
Elevation	950 m H_2O (9.3136 E+6 Pa)
Pressure head	0 m H_2O (0 Pa)
Total head	950 m H_2O (9.3136 E+6 Pa)
Temperature	23.8 C
Point D (above water table)	
Elevation	925 m H_2O (9.0685 E+6 Pa)
Pressure head	−30.6 m H_2O (3 E+5 Pa)
Total head	894.4 m H_2O (8.7685 E+6 Pa)
Saturation – matrix	80%
Saturation – fracture	80%
Temperature	23.8 C
Point D (below water table)	
Elevation	925 m H_2O (9.0685 E+6 Pa)
Pressure head	0 m H_2O (0 Pa)
Total head	925 m H_2O (9.0685 E+6 Pa)
Temperature	23.8 C
Point E	
Elevation	−50 m H_2O (4.9019 E+5 Pa)
Pressure head	1100 m H_2O (1.0784 E+7 Pa)
Total Head	1050 m H_2O (1.0294 E+7 Pa)

Table C-1. Summary of parameter values for the tuff geologic setting conceptual model (Cont'd)

Property	Value
Temperature	48.8 C
Point F	
Elevation	−75 m H_2O (7.3529 E+5 Pa)
Pressure head	1100 m H_2O (1.0784 E+7 Pa)
Total head	1025 m H_2O (1.0049 E+7 Pa)
Temperature	48.8 C
Point G	
Elevation	−100 m H_2O (9.8038 E+5 Pa)
Pressure head	1150 m H_2O (1.1274 E+7 Pa)
Total head	1050 m H_2O (1.0294 E+7 Pa)
Temperature	48.8 C
Point H	
Elevation	−125 m H_2O (1.2255 E+6 Pa)
Pressure head	1150 m H_2O (1.1274 E+7 Pa)
Total head	1025 m H_2O (1.0049 E+7 Pa)
Temperature	48.8 C

Table C-2. Parameter value ranges and document sources for tuff geologic setting. Document sources are: (1) Isherwood (1981), (2) Mercer et al. (1982), (3) Weast (1981), (8) Freeze and Cherry (1979), (9) NRC (1993), (10) Guzowski et al. (1983), and (11) Tien et al. (1985).

Property	Range	Document Source	Representative Value	Document Source
Saturated hydraulic conductivity - matrix	2.4 E-14 - 2.7 E-5 m/s	9	6.3 E-11 m/s	9
Saturated hydraulic conductivity - fracture	3.8 E-10 - 8.2 E-3 m/s	9	1.5 E-9 m/s	9
van Genuchten α - matrix	0.0006 - 0.06 1/m	9	0.006 1/m	9
van Genuchten α - fracture	-	-	1.3 1/m	9
van Genuchten β - matrix	1.2 - 10.6	9	1.8	9
van Genuchten β - fracture	3.2 - 5.3	9	4.2	9
Porosity - matrix	6 - 65%	9	10%	9
Porosity - fracture	0.0013 - 0.18%	9	0.004%	9
Effective porosity - matrix	3 - 15%	11, p 140	5%	11, p 141
Density	2230 - 2630 kg/m^3	9	2580 kg/m^3	9
Dispersivity	0.3 - 30 m	9	6 m	9
Thermal conductivity	0.64 - 2.77 W/m-C	10, p 173	1.7 W/m-C	10, p 178
Specific heat	837 - 2090 J/kg-C	10, p 161	1150 J/kg-C	10, p 178
Thermal diffusivity	3.0 E-7 - 7.3 E-7 m^2/s	10, p 179	6.0 E-7 m^2/s	10, p 178

Table C-2. Parameter value ranges and document sources for tuff geologic setting (Cont'd)

Property	Range	Document Source	Representative Value	Document Source
Limestone				
Hydraulic conductivity	7 E-10 - 3 E-6 m/s	8, p 29	1 E-6 m/s	8, p 29
Porosity	0 - 20%	8, p 37	5%	8, p 37
Density	2680 - 2760 kg/m^3	3, p F1	2720 kg/m^3	8, p F1
Dispersivity - longitudinal	7 - 61 m	1 V1, p 211	20 m	1 V1, 211
Dispersivity - transverse	1 - 20 m	1 V1, p 211	4 m	8, p 400
Thermal conductivity	1.97 - 3.35 W/m-C	2, p 118	3.60 W/m-C	2, p 119

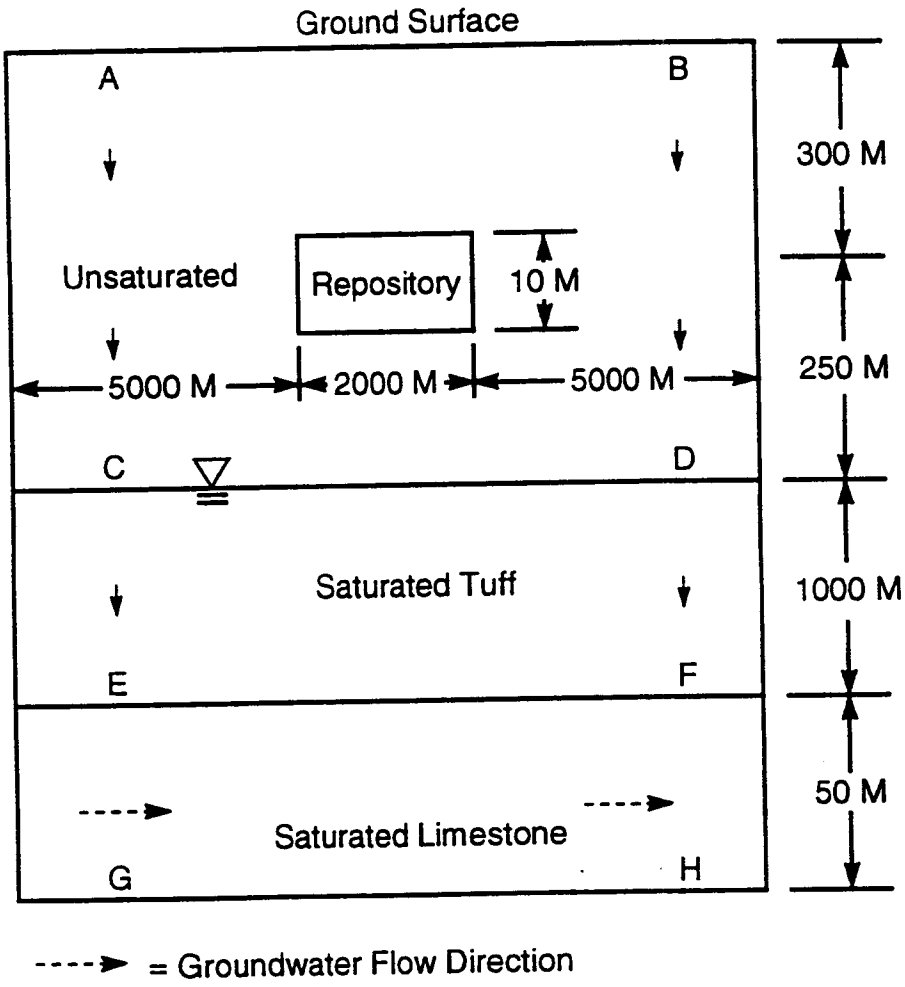

Figure C-1. Tuff geologic setting conceptual model